U.S. GEOLOGICAL SURVEY LIBRARY
CLASS

(200)
R290
no.80-185

USGS LIBRARY-RESTON
3 1818 00072847 5

UNITED STATES DEPARTMENT OF THE INTERIOR

GEOLOGICAL SURVEY

INTRUSIONS AND INTRUSIVE COMPLEXES IN AN OPHIOLITE NEAR SAN LUIS OBISPO: A CHEMICAL AND PETROLOGIC STUDY

By

Jane E. Nielson Pike

Open-File Report

80-185

U.S. GEOLOGICAL SURVEY
RESTON, VA.
DEC 02 1980
LIBRARY

U.S. Geological Survey
Reports-Open File Series

This report is preliminary and has not been edited or reviewed for conformity with Geological Survey standards or nomenclature

"The combination of causes of phenomena is beyond the grasp of the human intellect. But the impulse to seek causes is innate in the soul of man. And the human intellect, with no inkling of the immense variety and complexity of circumstances conditioning a phenomenon, any one of which may be separately conceived of as the cause of it, snatches at the first and most easily understood approximation, and says here is the cause."

Lev Tolstoy

ACKNOWLEDGEMENTS

Financial support for this study was provided by the Stanford Shell-Esso Research Fund, the American Federation of Mineralogical Societies and two Stanford Department of Geology Fellowship awards. Wet-chemical analyses were contributed by the Universidad Autonoma de Mexico and performed by Alberto Obregon, analyst.

I am indebted to Dr. Benjamin M. Page for his suggestion of this ophiolite body as a subject of intensive chemical study. His generous contribution of samples, thin sections and time in the field provided invaluable background for this work. Equally valuable were numerous discussions at all stages of the research. Dr. K. B. Krauskopf materially aided in defining the problem and developing the direction of the research. Discussions with Dr. W. C. Luth provided many insights into petrographic textural interpretations and the problems of defining paths of crystallization. Drs. J. G. Liou, R. R. Compton and H. G. Wilshire also contributed substantially to my thinking in developing interpretations of the San Luis Obispo data.

Collection and reduction of electron probe data would have been impossible without the unstinting support, advice and rescue efforts of Dr. Kenneth L. Williams. His suggestion that whole-rock analyses could be made using electron probe techniques and his efforts to produce a working probe automation system provided the bulk of rock analyses included in this report.

In addition, I thank numerous people for deepening and broadening my thinking in many directions. The most notable contributions came from discussions with: R. C. Evarts and A. W. Snoke on ophiolites, P. E. Long on geologic, petrologic and political topics and W. E. Dibble on geochemistry and crystal growth. Special recognition must be accorded R. C. Ewing for his tireless efforts to reorient my scientific and philosophical outlooks toward genteel paranoia and dynamic skepticism.

Lastly, but most, I acknowledge the patience and loyalty of R. J. Pike and B. R. Pike who assisted in the field and endured the long absences while lab work was completed. In addition, R. J. Pike fearlessly edited this manuscript. This support has made everything worthwhile.

TABLE OF CONTENTS

	Page
LIST OF TABLES	ix
LIST OF FIGURES	xi
ABSTRACT	xiv
I. INTRODUCTION	1
II. ALPINE ULTRAMAFIC ROCKS AND OPHIOLITE	4
Alpine Ultramafic Rocks	4
The Ophiolite Suite	6
Ophiolites and Oceanic Crust-Mantle	8
Thickness of ophiolites	13
Alkalic nature of ophiolite lavas	13
Ultramafic rocks of ophiolites	14
Rocks Associated with Ophiolites	15
III. SAN LUIS OBISPO OPHIOLITE	16
Regional Geologic Setting	16
Geology of the Ophiolite	18
IV. COMPOSITIONAL RELATIONS IN THE SAN LUIS OBISPO OPHIOLITE HOST ROCKS	23
Ultramafic and Volcanic Units of the San Luis Obispo Ophiolite	23
The basal ultramafic unit	23
Diabasic dikes intruding the basal ultramafic layer	39
The volcanic unit	49
Summary	66
V. THE INTRUSIVE COMPLEXES	68
Cerro Alto Intrusive Complex	68
Cuesta Ridge Intrusive Complex	79
Gabbroic rocks of the Cuesta Ridge intrusive complex	84
Felsic rocks of the Cuesta Ridge intrusive complex	92
Diabasic rocks of the Cuesta Ridge intrusive complex	112
Breccias in the Cuesta Ridge intrusive complex	116
Summary	127

Page

VI. CHEMISTRY AND ALTERATION OF THE SAN LUIS OBISPO OPHIOLITE 131

Chemical Relations Among Rocks of the San Luis Obispo Ophiolite 132
Effects of Metamorphism on Ophiolite Chemistry 141
Conditions of Greenschist Facies Metamorphism 143
Summary 150

VII. CONCLUSIONS 152

Model of Ophiolite Formation 153
Remaining Problems 156

APPENDICES 158

I. ELECTRON PROBE MICROANALYSES OF MINERALS 159

a. Pyroxenes 161
b. Amphiboles 163
c. Plagioclases 180
d. Chlorites 189
e. Epidotes 196

II. WHOLE ROCK ANALYSES OF ROCKS BY ELECTRON PROBE 200

REFERENCES 205

LIST OF TABLES

Table		Page
1a.	Whole Rock Analyses of Ultramafic Rocks of the San Luis Obispo Ophiolite	26
1b.	Whole Rock Analyses of Diabasic Rocks from the San Luis Obispo Ultramafic Unit	27
2a.	Electron Probe Analyses of Olivines from a Cumulate Ultramafic Xenolith	31
2b.	Fo Content of Olivines in Cumulate Complexes	31
3.	Electron Probe Analyses of Amphiboles from Diabases Intrusive into the Ultramafic Unit	44
4.	Ratios of Calcium to the Octahedral Ions which form Minerals in Rodingitization	47
5a.	Whole-Rock Analyses of Spilitized Basaltic Lavas . . .	52
5b.	Whole-Rock Compositions of Average Fresh Basalt and Average Greenstone from Latitude 22° N., Mid-Atlantic Ridge (MAR)	53
6.	Modes of Spilitized Lava and Intrusion	55
7.	Optical Determination of Pyroxenes in Spilitized Lavas	56
8a.	Composition of Greenstones Compared to Average of Fresh Abyssal Basalts Dredged from the Mid-Atlantic Ridge (MAR)	61
8b.	Differences Between MAR Average Greenstone and Spilites of the San Luis Obispo Ophiolite	62
9.	Modes of Amphibolite and Uralite Gabbro	73
10.	Compositions of Amphibolites and Uralite Gabbros of the Cerro Alto Intrusive Complex	75
11a.	Diabasic Intrusions of the Cuesta Ridge Intrusive Complex	82

Table Page

11b. Gabbros in the Cuesta Ridge Intrusive Complex 83

12. Modal Compositions of Rocks in the Cuesta Ridge Intrusive Complex 85

13. Electron Probe Analyses of Plagioclase in Upper Gabbro Mass, Cuesta Ridge Complex 91

14. Felsic Rocks of the Cuesta Ridge Intrusive Complex 99

LIST OF FIGURES

Figure		Page
1.	Comparison sections of ophiolites with ocean crust and mantle thicknesses and seismic velocities	11
2.	Location and setting of the San Luis Obispo ophiolite	17
3.	The San Luis Obispo ophiolite	19
4.	Bastite texture in sheared ultramafic rock	24
5.	AFM diagram of ultramafic rocks and diabasic intrusions of the basal ultramafic layer	28
6.	Cumulate textures	30
7.	Analyzed pyroxenes plotted on pyroxene quadrilateral	33
8.	Compositions of amphiboles in ultramafic rocks and intrusive diabases	34
9.	δD-δO^{18} diagram comparing oceanic serpentinite with ophiolite serpentinite	37
10.	Diabasic dikes in the basal ultramafic unit	42
11.	Structures in spilite lavas	51
12.	Spherulitic devitrification texture in formerly glassy spilite	59
13.	AFM diagram of spilitized lavas	60
14.	Ti-Zr plot of Pearce and Cann (1971)	65
15.	Cerro Alto intrusive complex	69
16.	Amphibolite textures in rocks of the Cerro Alto intrusive complex	72
17.	Amphibolite compositions in amphibolite and uralite gabbro, Cerro Alto intrusive complex	74

Figure | Page

18. AFM diagram of rock compositions from the Cerro Alto intrusive complex 76

19. Cuesta Ridge intrusive complex 78

20. Cumulate gabbro 81

21. Amphibole compositions from gabbros in the Cuesta Ridge intrusive complex 87

22. AFM diagram of rocks from the Cuesta Ridge intrusive complex 88

23. Multistage textures in gabbro 90

24. Contact relations among Cuesta Ridge complex intrusions 94

25. Variation of composition with vertical position for felsic sills of the Cuesta Ridge intrusive complex 97

26. AFM diagram of felsic rocks in the Cuesta Ridge intrusive complex 100

27. Metamorphic textures in albite-chlorite "diorite" . . 102

28. Composition of plagioclases in Cuesta Ridge intrusions 104

29. Chlorite compositions 106

30. Textures in quartz-diorite and quartz-albitite rocks 109

31. Textures of diabases in the Cuesta Ridge intrusive complex 114

32. Amphibole compositions in diabases of the Cuesta Ridge intrusive complex 115

33. Breccias formed at the contact between diabase dike and quartz-albitite sill 117

34. Breccia textures 120

35. Melt-textures in brecciated quartz-albitite 122

36. Breccia "porphyry" 126

37. Plastic deformation in brecciated sills of the Cuesta Ridge intrusive complex 129

Figure Page

38. Chemical variation of the San Luis Obispo ophiolite 135

39. Model of possible liquid and residua compositions produced from melting in a Cuesta Ridge gabbro 139

40. Stability fields in basic rocks 146

41. Stability limits of Ca-Mg amphiboles 148

42. Stability limits of epidotes 149

43. Stages in formation of the San Luis Obispo ophiolite 154

ABSTRACT

The San Luis Obispo ophiolite is a sequence of mafic and ultramafic rocks that lie as a thrust-like slice on top of Franciscan mélange in the southern California Coast Range. The ophiolite comprises the classic Steinmann Trinity of basal serpentinized ultramafic rocks overlain sequentially by spilitized pillow lavas and cherts. The ophiolite is intruded by numerous diabasic dikes and several large intrusive complexes that contain peridotite, gabbro, diabase and felsic rocks.

Field relations indicate that this ophiolite originated as a sequence of submarine volcanic flows and breccia units extruded onto an ultramafic basement. Later the volcanic and ultramafic rocks were intruded along their contact by mafic magma that crystallized as a stratiform complex of cumulate peridotite and gabbro. Next, this stratiform complex was intruded by diorite and albite-granite (trondhjemite) sills, which may have been produced by partial melting of gabbros in the upper levels of the stratiform complex. Finally all earlier units were intruded by diabasic sills and dikes that probably were late feeders for the pre-existing volcanic unit. All the ophiolite rocks underwent subsequent highly localized brecciation, under greenschist-facies conditions, in which felsic rocks were incipiently melted by frictional heating.

The host rocks and intrusions were metamorphosed at low temperature and the mafic rocks were altered by Na- and Si-metasomatism.

Despite this pervasive alteration, evidences of the formational stages of the ophiolite are preserved in disequilibrium mineral assemblages, primarily within mafic and ultramafic rocks of the intrusive complexes. Whole-rock analyses of the ophiolite suite indicate that alteration has obscured but not obliterated the original chemical character of the mafic rocks. The ophiolite diabases and basalts contain up to 6 weight percent Na_2O and 58 percent SiO_2, in contrast to normal SiO_2 contents of 50 percent or less and Na_2O contents of less than 3 percent for unaltered oceanic and continental tholeiite basalts. However, the low K_2O contents (less than 0.8 percent) of all units in the ophiolite suite indicate that these rocks are not part of an alkalic kindred, but rather are altered tholeiites.

Compositions of relict amphibole and plagioclase in the mafic rocks indicate that the ophiolite formed in a high-temperature environment and the deep seated rocks were metamorphosed under amphibolite-facies conditions. A later change in the environmental conditions allowed subsequent low-temperature (greenschist facies) metamorphism and metasomatism. The structure and chemistry of the San Luis Obispo ophiolite support the hypothesis that this body may represent a fragment of oceanic crust and mantle. The volcanic rocks and the intrusive complexes probably formed at a mid-ocean ridge, where conditions of high heat-flow provided the requisite high-temperature environment and promoted the production of mafic magmas. The change to low-temperature conditions probably was due to inception or acceleration of crustal spreading at that portion of the ridge where this ophiolite formed. The nature of brecciation in the ophiolite indicates that the low-temperature environment also was one of greater

tectonic disturbance, relative to conditions at the ridge. This tectonically active environment probably corresponds to an island arc where the ophiolite-bearing plate was subducted in an adjacent trench. The absence of a high-pressure mineral assemblage in the San Luis Obispo ophiolite suggests that this segment of ocean-crust and upper mantle was not buried in a subduction zone, but rather was rafted on top of subduction mélange (Franciscan Formation) into its present position.

CHAPTER I

INTRODUCTION

Isolated blocks and extensive sequences of ultramafic and mafic rocks occur frequently in the California Coast Range, but because the importance of these rocks was recognized only recently, their petrologies and chemical compositions have not been examined in detail. Fragments of ultramafic rocks (usually serpentinites) in association with pillowed basaltic lavas, now are believed to mark the worldwide zones of intense tectonic activity. These mafic and ultramafic rock sequences are called ophiolite. In the California Coast Range ophiolites may be fragments of the ocean crust and mantle, derived from a subducted oceanic plate during collision with the margin of a continental crustal plate (collision of the North American and East Pacific Plates, Atwater, 1970).

Until recently, the geology of the mafic and ultramafic rocks, in Jurassic-Cretaceous Franciscan rocks of the California Coast Range near Atascadero, was largely unknown. Fairbanks (1904) mapped the San Luis Obispo area at 1:125,000 and interpreted the ultramafic rocks as intrusive into Franciscan sediments and overlying volcanic rocks. Much later, Hsü (1969) mapped the Franciscan Formation in the Coast Range between Morro Bay and San Simeon as mélange and designated the pillow lavas and ultramafic rocks as ophiolite. Subsequently, Page (1972) mapped the synclinal segment of ophiolite that

is the subject of this study. Page determined the structural relations among the major ophiolite units and interpreted the ophiolite sequence as a fragment of oceanic crust that had been underthrust by the Franciscan mélange.

Interpretations of all ophiolite sequences worldwide have been based upon the structure of the masses, a few chemical data, and comparisons of the ophiolites with ocean crust structure and what is known of oceanic rock compositions. Until recently, detailed chemistry has not been obtained for any ophiolites (Hopson and Frano, 1973).

Deformation and metamorphism have pervasively affected the major rock types in most ophiolites, although primary mineral relics can be found in portions of the rock sequence. Detailed investigation of the mineral relics and determination of the style of chemical alteration in these rocks is necessary before genetic interpretations of ophiolite formation can be made. This study is a detailed examination of mineralogy and whole-rock chemistry of the San Luis Obispo ophiolite, with special attention to the various intrusive rocks.

Mineral identifications in 200 thin sections were made using conventional petrographic techniques, as well as from universal stage and x-ray diffraction identifications of selected samples. Compositions of 368 individual minerals, representing six mineral groups, were obtained with electron probe microanalyzer. Ten wet-chemical analyses were kindly donated by agreement with the Universidad Autonoma de Mexico, and 63 rapid whole rock analyses were performed by electron probe. Semi-quantitative determinations of selected trace elements were obtained commercially.

These data establish a chemical relationship among the host and intrusive rocks of the San Luis Obispo ophiolite. Alteration trends can also be established for most of the rock types. Textural data from the intrusive rocks yield important information on the tectonic setting in which this ophiolite was formed.

CHAPTER II

ALPINE ULTRAMAFIC ROCKS AND OPHIOLITE

Alpine Ultramafic Rocks

Ultramafic and associated rocks are uncommon in the earth's crust. They occur principally in four associations, as suggested by Wyllie (1967):

1. stratiform mafic-ultramafic complexes such as Skaergaard (Wager and Brown, 1968), Stillwater (Hess, 1960; Jackson, 1961), Bushveld (Cameron, 1963), and Muskox (Irvine and Smith, 1967)

2. xenolithic fragments in basalt flows of Hawaii (Kuno, 1967; Jackson, 1967), the southwestern U. S. (Wilshire, et al., 1974) and Australia (Wilshire and Binns, 1961), and in kimberlite-bearing diatremes of South Africa and other parts of the earth's crust where deep-seated volcanism has occurred (Davidson, 1967)

3. concentrically zoned igneous bodies of alkalic affinities such as Kiglapait (Morse, 1969)

4. fragments, lenses or massive bodies in folded and faulted mountain belts (Hess, 1955). These are termed alpine-type ultramafic rocks.

The alpine ultramafic rocks are characterized chiefly by their tectonic setting, which includes association with mélange units, nappes, and other highly deformed structures (Moores, 1973). When unserpentinized, they often have oriented fabrics and lack the primary crystallization textures that characterize the stratiform and concentric complexes (Hess, 1955; Thayer, 1960). Although alpine ultramafic rocks often are layered, usually the layers are contorted and

discontinuous. This is in sharp contrast to the continuous layering of stratiform complexes such as Skaergaard, in which individual layers can be identified over distances of several kilometers. Alpine ultramafic complexes commonly are not bordered by a well-developed metamorphic aureole, which would be expected around the contacts of intrusive rocks with such high liquidus temperatures as dunite, peridotite and pyroxenite (O'Hara, 1967a). These circumstances suggest that, unlike the relatively undisturbed stratiform and concentric ultramafic-mafic bodies, the alpine-type ultramafic rocks have undergone a very complex history since formation.

The high density of the alpine ultramafic rocks and their characteristic tectonic setting have led to the widespread belief that these bodies are fragments of mantle. According to this hypothesis the mantle fragments have been squeezed into the base of the earth's crust during orogenesis (Hess, 1955) in the form of a relatively "cool" (i.e. subliquidus) crystal "mush," lubricated by serpentinization at the borders. A second hypothesis regards bodies of alpine ultramafic rock as stratiform or other zoned-type complexes that have been squeezed into overlying crust (Thayer, 1960) or underlying crust (McTaggart, 1971). This idea followed from Thayer's observation at Canyon Mountain, Oregon (1963), and other areas that gabbros and other feldspathic rocks often form part of the alpine "ultramafic" complex.

Yet another hypothesis (Osborn, 1969) holds that alkali basalt, generated in a mobile belt, differentiates to form the "complements" extrusive andesite and hypabyssal cumulate ultramafics. The ultramafics are later emplaced into higher crustal levels and tectonically

1. The euhedral plagioclase is roughly equant, and its formerly square outlines and twinning are discernible. The present boundaries are complex and sutured, as illustrated in figure 27a

2. The chlorites occur in clusters that resemble aggregates of rounded shapes, rather like clusters of grapes (fig. 27b). Rare relict garnets are associated with the chlorite clusters (fig. 27c).

The whole-rock analysis 21 in figure 26 lies well within the field of diabasic rocks. Although the mafic origin of this rock still is apparent, its textures and mineralogy demonstrate that it has been altered. Thus, analysis 21 represents another rock in the sill complex with a multi-stage history. The history of formation includes a post-crystallization, high-temperature metamorphism (to a garnet-plagioclase assemblage, possibly in the almandine-amphibolite facies), and retrogressive metamorphism to chlorite + albite, with the addition of SiO_2 and loss of CaO. It is unclear whether or not Na_2O was added because all the rocks in the entire ophiolite, except ultramafic rocks, are rich in Na_2O. Once again, SiO_2 enrichment is due to metasomatic liquids from an unknown source.

Plagioclases in the felsic rocks have been pervasively altered. Figure 28 is a plot of electron probe analyses of plagioclase in the intrusive complex against their vertical position in the pile of sills. Although even the gabbros contain plagioclases with albite compositions, as illustrated in the figure, the alteration reactions never attained complete equilibrium, but left albitized basic rocks with relics of high-calcium plagioclase. Many diorites rich in epidote contain entirely albitized feldspars. Evidently, equilibrium was nearly attained in the alteration reactions and released calcium was

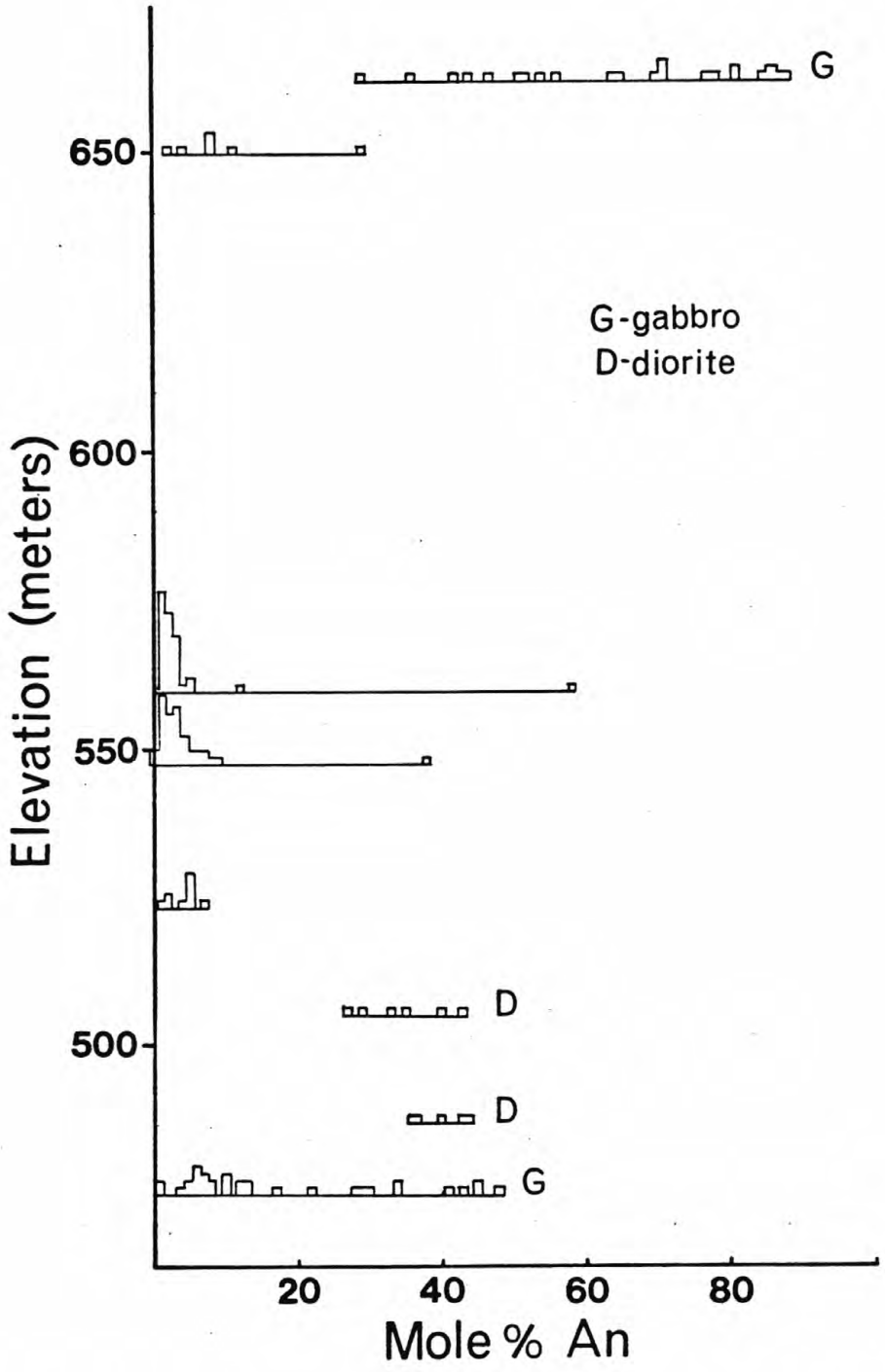

Fig. 28.--Composition of plagioclases in Cuesta Ridge intrusions.

quickly taken up into epidote. Epidote compositions (about Ps_{25}) are listed in Appendix Ie. The structural formulae indicate that the alteration produces stoichiometric epidotes.

K_2O contents of all the feldspars are very low and range from 0 to under 2 weight percent (Appendix Ic). There is no primary or secondary K phase in any rocks of the ophiolite. Ten quartz-albitites and diorites were stained for plagioclase and K-feldspar; none showed any yellow stains characteristic of the potassic phase. All the quartzo-feldspathic rocks of the complex were examined closely to determine whether K_2O might have been mobilized during alteration to form veins of K-feldspar and K-bearing micas as it escaped. However, no such veins were observed. Even the clays are rare in these rocks, and when present appear to be low-K smectites. If potassium was ever an abundant element in any of these rocks, it has since been efficiently removed.

Chlorites of the Cuesta Ridge intrusive complex are higher in silica than the unoxidized ripidolitic varieties normally found in greenschist-facies rocks (Wetzel, 1973). Electron probe analyses of Cuesta Ridge rocks are plotted in figure 31, in which all Fe is treated as Fe^{+2}. The Si values of ripidolite lie between 2.5 and 2.8 (Hey, 1956), but the Cuesta Ridge chlorites fall outside this range. The probe analyses cannot distinguish between Fe^{+2} and Fe^{+3} states; however, unoxidized chlorites with these Si contents are relatively rare. It therefore is reasonable to assume that the Cuesta Ridge intrusions contain oxidized chlorites since they then fall in the compositional range of chamosite on figure 29a (Hey, 1956). The same chlorites are plotted in figure 29b, which shows their high

CHLORITE COMPOSITIONS

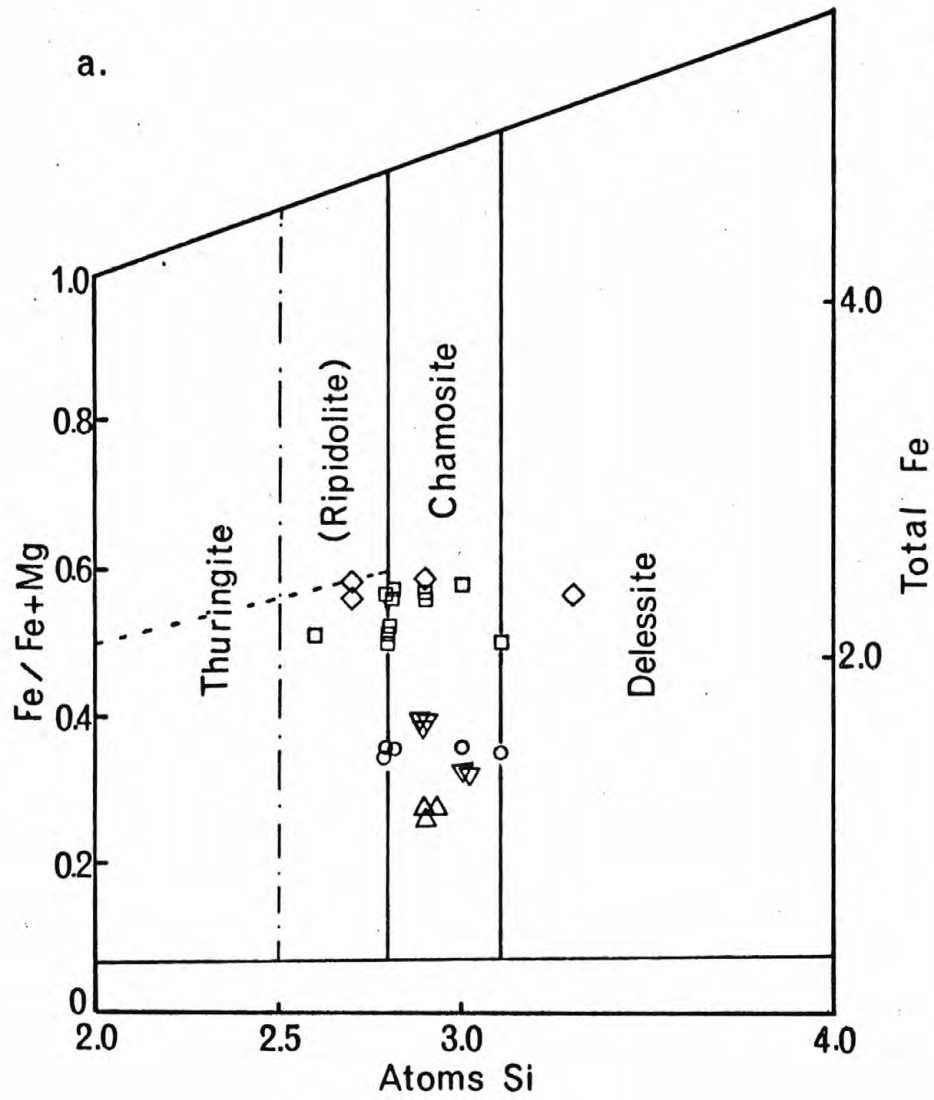

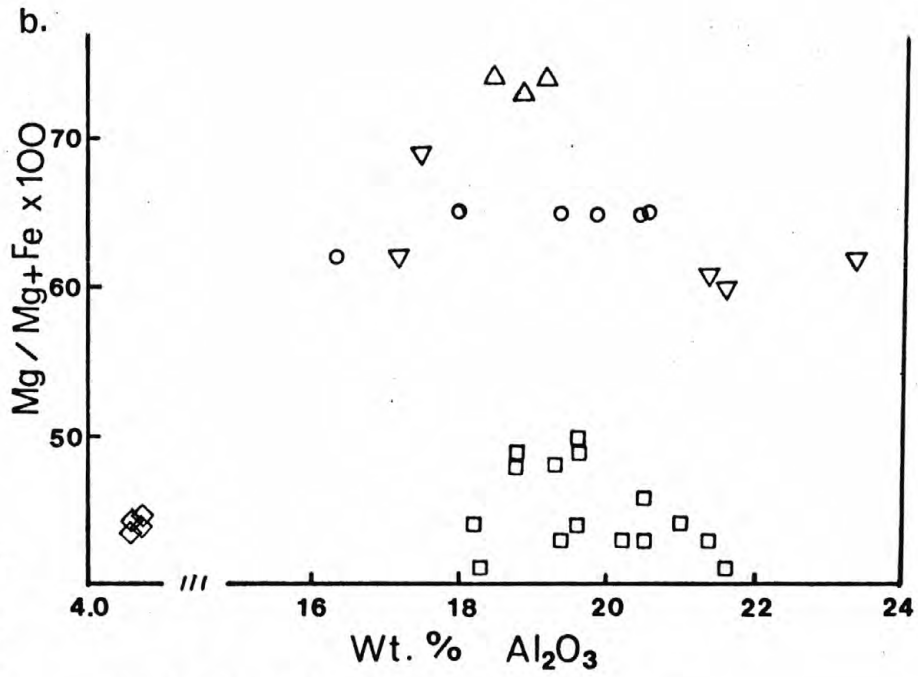

SYMBOLS (data in Appendix Id)

- ○ diabase - table A-1
- △ " " A-2
- ▽ diorite " B
- □ " " C-1
- ◇ " " C-2

Fig. 29

aluminum contents. Those chlorites from mafic rocks (such as 21, table 14; 10, 11, table 11) are clearly separated from the felsic rock chlorites by their high Mg/Mg+Fe ratios.

Three textures in the felsic rocks furnish important clues to the late-stage formation of the Cuesta Ridge intrusive complex. The quartz-diorites are often coarsely variolitic or else are hypidiomorphic-granular; rarely they contain plagioclase-quartz intergrowths. Quartz-albitites are either hypidiomorphic-granular or have quartz-albite intergrowths that resemble granophyre.[1] These textures are illustrated in figure 30.

The variolites often are coarse-grained and contain elongate former actinolites, now altered to chlorite. The varioles usually are "bow-tie" in form, rather than having developed a complete radial pattern (fig. 30a, b). In hand specimen, these rocks have an appearance of criss-crossing straws. This "jackstraw" texture may reflect the formation of a few spherulite nucleation centers because of initial undercooling to a temperature close to the system liquidus (Fenn, 1973). Following initial nucleation, the cooling would have progressed slowly, allowing annealing of the incipient spherulites to solid plagioclase laths and coarsening of grain size.

Hypidiomorphic-granular textures (fig. 30c, d) probably are due to formation of few, well-spaced nuclei and reflect slow cooling during the entire crystallization history of these rocks. The slow

---

[1]"Granophyre" is a term that many petrologists use in a compositional sense to mean intergrowths of K-feldspar or alkali-feldspar and quartz. "Myrmekite" is used for intergrowths of plagioclase and quartz, but this also is used to indicate a vermiform type of intergrowth. The quartz-albite intergrowths in the Cuesta Ridge felsic rocks more closely resemble granophyre than myrmekite in texture.

Textures in Quartz-Diorite and Quartz-Albitite Rocks

Fig. 30--(a) variolite texture. Crossed polarizers, 1 in. = 3 mm.

(b) one "bow-tie" plagioclase intergrowth in variolite rock. Crossed polarizers, 1 in. = 0.4 mm.

(c) granophyric textures. Crossed polarizers, 1 in. = 0.4 mm.

(d) hypidiomorphic granular texture with coarse subhedral plagioclase (corroded) and anhedral quartz. Crossed polarizers, 1 in. = 0.4 mm.

(e) hypidiomorphic-granular texture with marginal granophyric zones around plagioclase grains. Crossed polarizers, 1 in. = 0.4 mm.

(a)

(b)

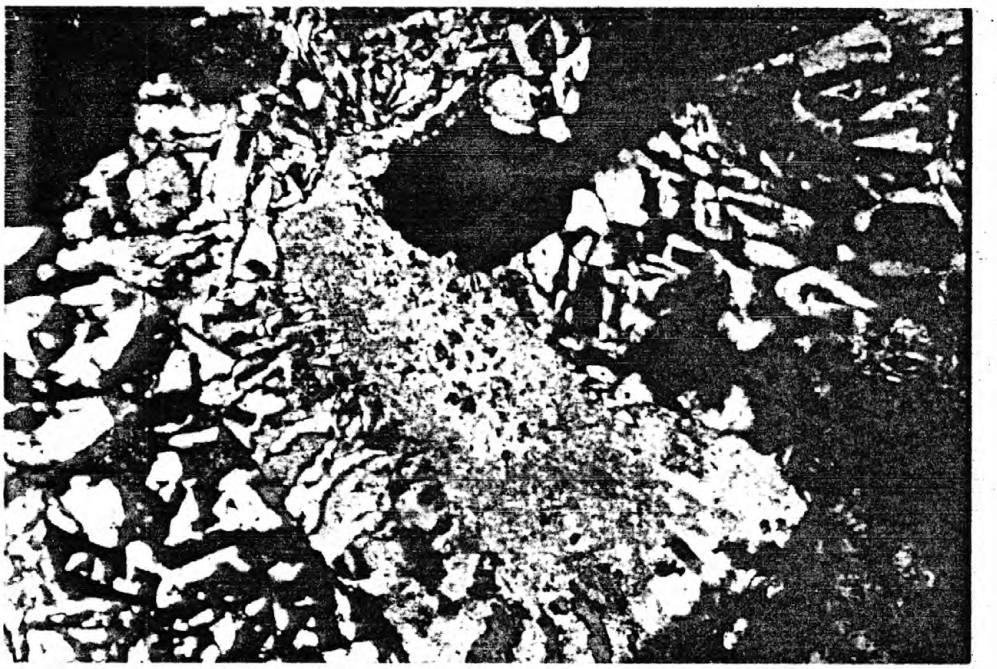

(c)

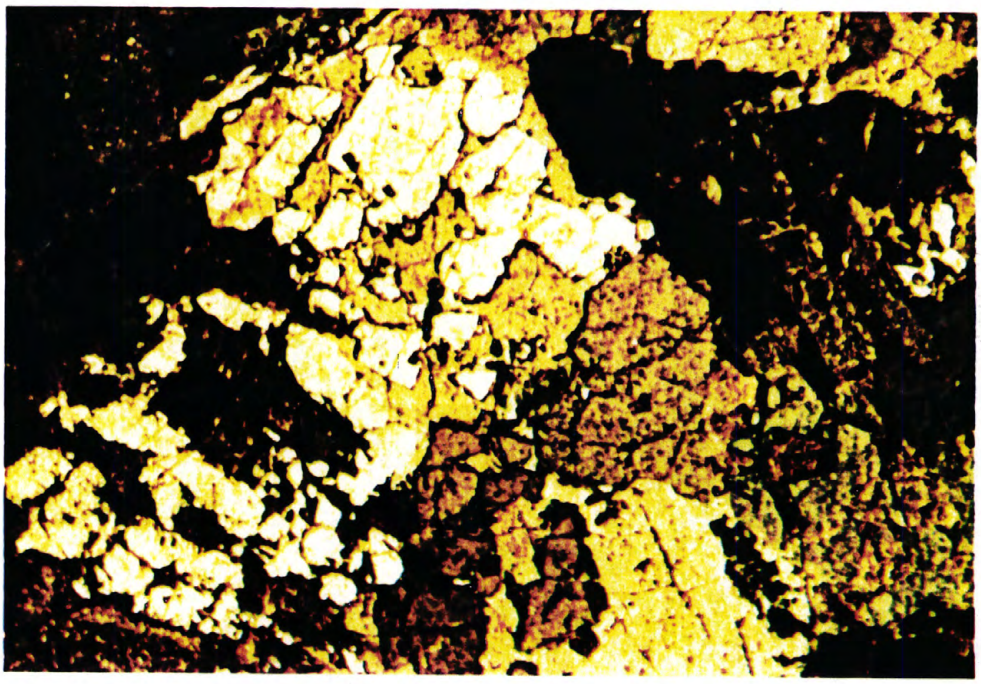

(d)

(e)

cooling allowed plagioclases to form coarse tabular crystals with coarse anhedral quartz concentrated in the interstices. Occasionally the last crystallization stages are represented by small amounts of granophyric intergrowth bordering the large plagioclase grains (fig. 30d). Accordingly, the last cooling stage of these rocks probably was quite rapid and produced this quench-texture.

The dominantly granophyric textures (fig. 30e) are produced by the quenching of rocks in which coarse plagioclases had begun to crystallize. The intergrowths developed as spherulitic crystals that nucleated on the planar faces of growing crystals when cooling of the rock accelerated. Lofgren (1974) has shown that the development of spherulitic textures is directly related to undercooling of the crystallizing liquids in unary and binary systems, although the relationship is not as strong in more complex systems. Spherulite development is complex and the mechanism of growth is not well understood for silicate systems. In simple terms, such crystals appear to form by rapid growth at the tips of nucleated crystals. Branching may occur along the growing crystal and impurities are ponded between the branches (Keith and Padden, 1963; Lofgren, 1968). Intergrowths of the granophyric type consist of feldspar crystals that have ponded quartz between the branching crystals. Thus the granophyric quartz-albitites are the felsic rocks of the Cuesta Ridge complex that appear to have cooled the most rapidly in the final stages.

Textures in the Cuesta Ridge intrusive complex suggest the following formational history of the sills:

1. initial slow crystallization of a stratiform mafic-ultramafic complex
2. metamorphism in portions of the mafic complex at high temperature and local melting.

The diorite and quartz-albitite rocks may have been the products of this partial fusion. The temperature must have continued high during the intrusion and cooling of the quartz-diorites and during much of the cooling of quartz-albitite sills. Finally, late-stage cooling proceeded rapidly, quenching the last stages of quartz-albitite crystallization. At this stage, the entire sequence of sills was altered deuterically. The late rapid cooling may have been caused by:

1. the lowering of the ambient temperature for the whole sequence of rocks
2. lowering of pressure on the complex
3. introduction of water into environment in which the complex formed.

Diabasic rocks of the Cuesta Ridge intrusive complex

Diabasic bodies also intruded the Cuesta Ridge sill complex late in its history. Due to brecciation along diabase-albite contacts (discussed below), it is unclear whether all or most of the diabasic sills are later than quartz-albitite. The diabasic dikes are the only rocks which cross-cut the major structures of the intrusive complex; these may represent apophyses from the larger (1-3 m thickness) diabase sills (fig. 24d). Also, the dikes occasionally have chilled margins, which means that they probably are the last rocks intruded into the pile of sills.

Diabasic sills and dikes in the Cuesta Ridge complex have two distinct textural habits, both of which are developed in greenschist-facies mineralogy:

1. relict diabasic textures of sub-ophitic laths of albite, which are intergrown with tremolite or actinolite, within a groundmass of chlorite + epidote ± quartz. Opaques and sphene occur as accessories in these rocks (table 19). Many mafic rocks of diabasic texture also contain rare plagioclase phenocrysts, now albitized.

2. metamorphic textures in which all grains are subhedral to anhedral. The mineralogy is dominated by chlorite + actinolite + epidote and the rock is often veined with prehnite. In these rocks, the phenocrysts were pyroxenes, now pseudomorphed by actinolite and chlorite, which form a characteristic spotted appearance in hand specimen.

Figure 31 illustrates both textural types.

The diabases, like all other rocks of the ophiolite, retain their mafic compositions in spite of pervasive low-temperature metamorphism. Their compositions (7, 8, 9, 10, 11, 12, table 11a) are rich in SiO_2 and Na_2O and low in CaO compared to the average basalts (L, M. table 1b). However, the Cuesta Ridge diabases cluster tightly within the field of basaltic rocks on an AFM plot (fig. 22). This compositional similarity suggests that the diabasic intrusions may have been portions of liquid from the same melting event that were intruded at about the same time.

The diabase's mineral assemblage contains rare relics of primary minerals within the greenschist-facies minerals. Compositions of two pyroxenes are about $En_{51}Fs_{22}Wo_{26}$ for the unaltered cores of chloritized phenocrysts in sample 9 (table 11). The electron probe analyses of these minerals are listed in Appendix Ia and plotted in figure 7 (Supra p. 33). These original minerals were chloritized after having been hydrated at high temperatures to hornblende. Compositions of some preserved hornblendes with high Al^{IV} contents are plotted in figure 32a. The figure demonstrates that most of the amphiboles have become actinolite and tremolite because of low-temperature metamorphism.

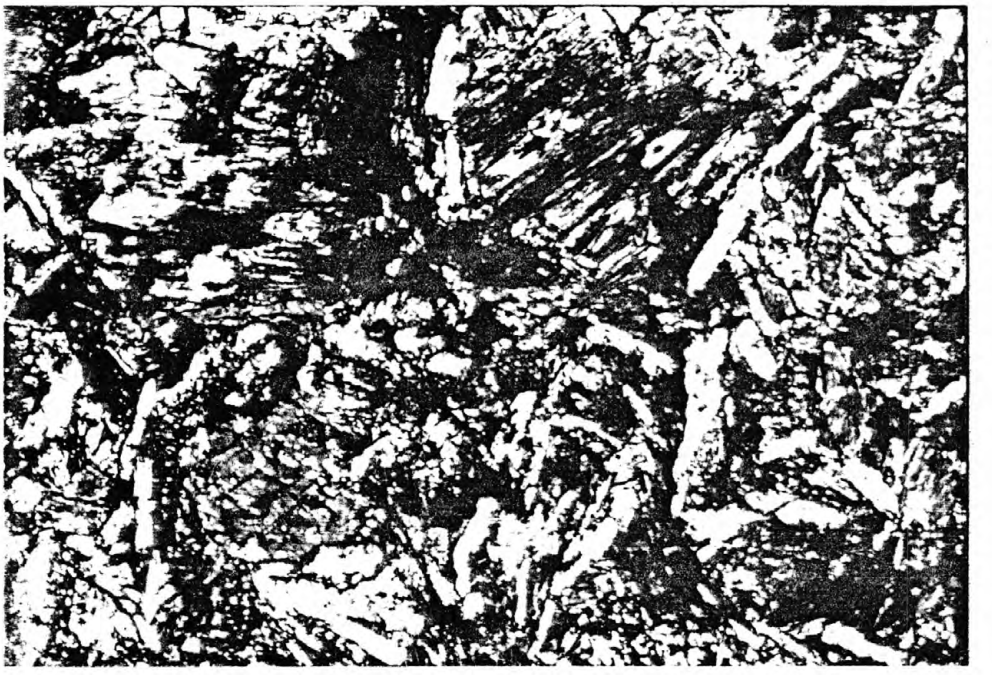

(a)

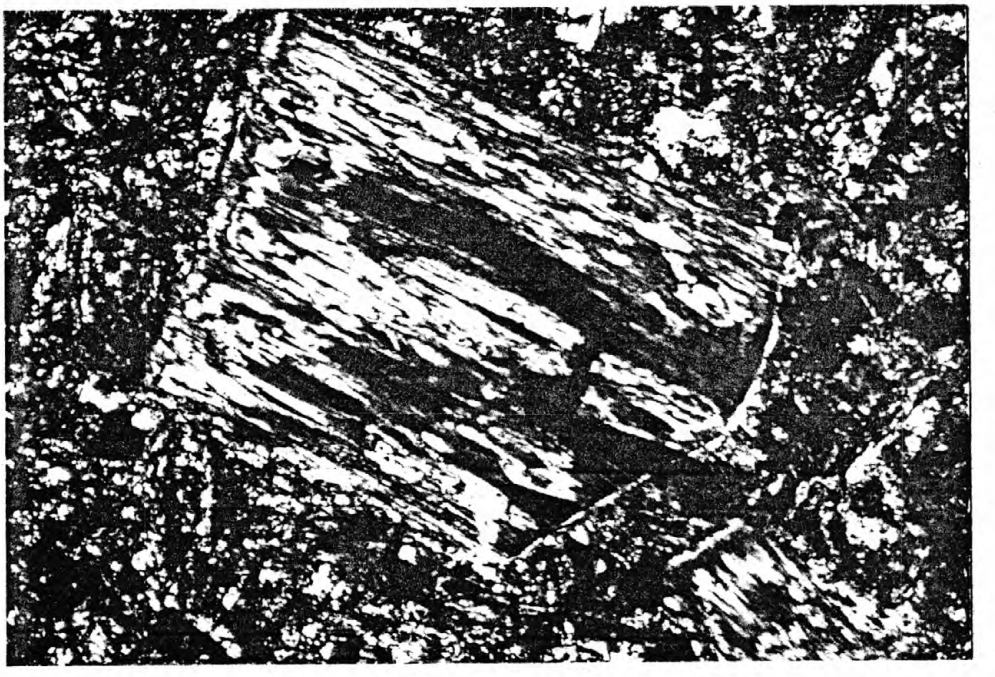

(b)

Textures of Diabases in the Cuesta Ridge Intrusive Complex

Fig. 31.--(a) relic equigranular diabasic texture

(b) tremolitized-chloritized pyroxene phenocryst in metamorphic-textures diabase

Crossed polarizers, 1 in. = 0.4 mm.

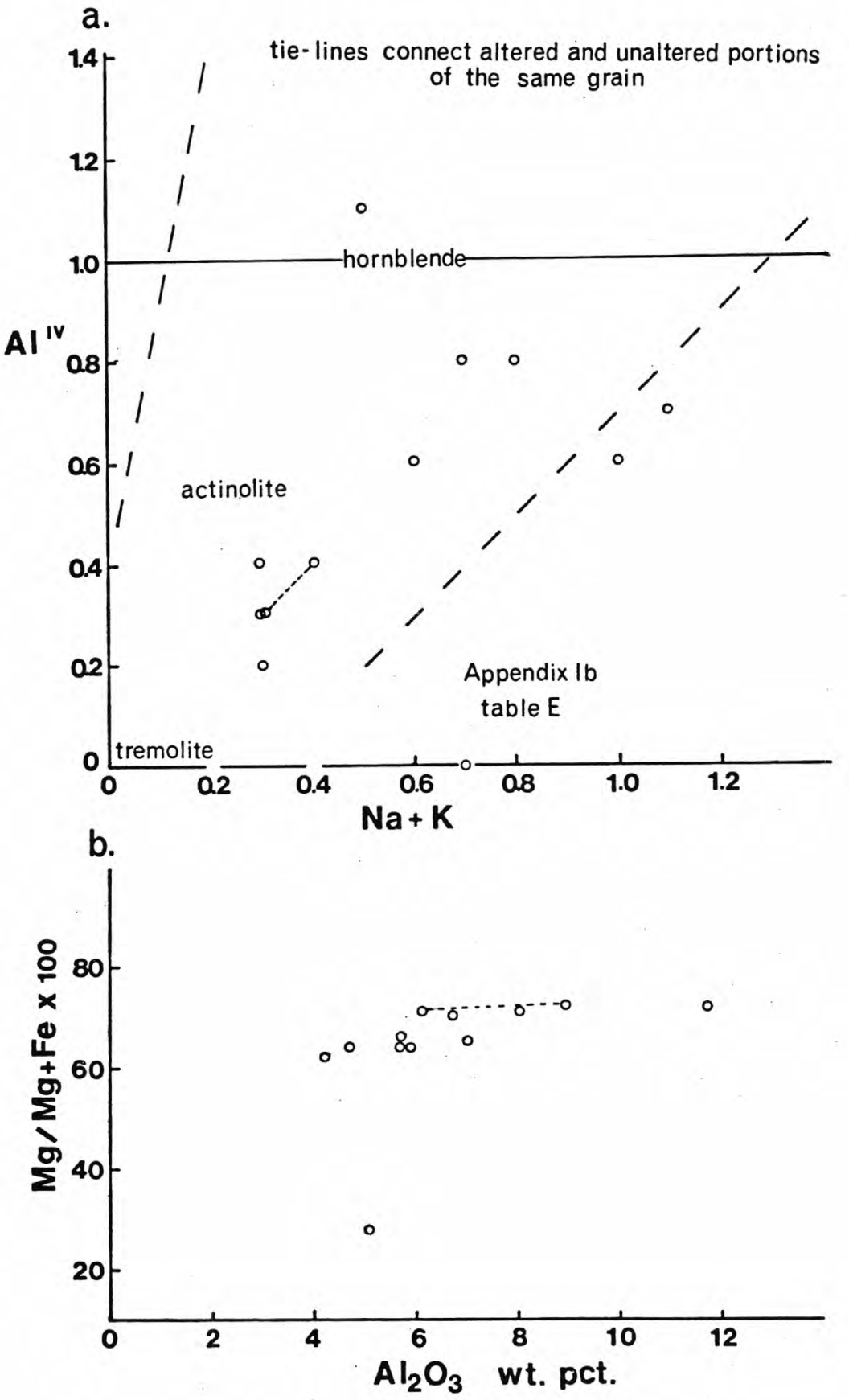

Fig. 32.--Amphibole compositions in diabases of the Cuesta Ridge intrusive complex.

All the amphiboles are high in Mg (fig. 32b), again reflecting derivation from magnesian pyroxene.

Chlorites from several diabases also show highly magnesian compositions (fig. 29) relative to chlorites of the felsic intrusions. These chlorites are probably oxidized, since they cluster in the area of chamosite.

Breccias in the Cuesta Ridge intrusive complex

Breccia textures occur in diabasic and felsic rocks throughout the Cuesta Ridge intrusive complex. Although brecciation usually is localized at sill-sill or sill-dike contacts (especially at contacts between diabase and quartz-albitite intrusions), it may also occur within massive diabase bodies. Felsic breccias often are difficult to recognize in outcrop, especially if brecciation is extensive. However, these occasionally stand out because they tend to be hard, flinty and more resistant to erosion than the unbrecciated rock. In contrast, diabasic breccias are readily recognizable in outcrop as friable rock with fragmental texture. Both types of breccia often are offset along high-angle faults of small displacement that transect intrusive contacts.

All of the breccias examined in this study are of the same composition as their host rocks. Even where rocks are brecciated on both sides of a felsic-mafic intrusive contact (fig. 33), there is no mixing of the two rock types. None of the breccias studied within this complex contains any exotic fragments derived from more distant rock types. The textures of the breccias are characterized by progressive breakdown of the rock into sheared zones that surround residual

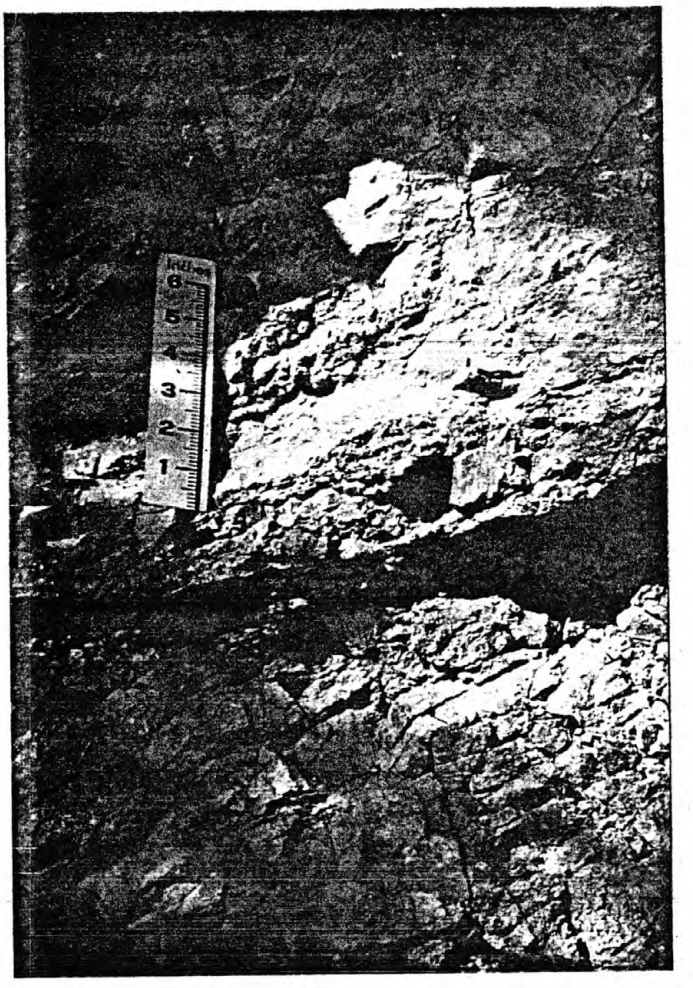

Fig. 33--Breccias formed at the contact between diabase dike and quartz-albitite sill. Note that the lower contact is still sharp even though rocks on either side are broken.

domains of original crystalline texture (fig. 34a). Quartz is frequently recrystallized into fine unstrained grains that have complex, sutured boundaries and are intergrown with epidote + chlorite in the sheared matrix (fig. 34b). In a few rocks, spherulitic crystallization of feldspar and quartz has developed within the brecciated zones. All stages of breccia development can be detected in the sheared rocks. This sequence begins with incipient fracturing within interstitial granophyric areas and strained quartz grains, passes through crumbling of grain boundaries (fig. 34c), and finally leads to development of sheared zones around relict domains to totally sheared and recrystallized zones.

Several lines of evidence suggest that the breccias formed in a moderate-temperature, low-pressure (greenschist facies) environment during a tectonic event that sheared rocks on a highly localized scale:

1. formation of epidote in the sheared matrix from the reaction plagioclase + Fe-Mg minerals + excess SiO_2 = epidote + chlorite + quartz

2. annealing of strain in quartz with no preferred orientation, and annealing of the felsic breccias to resistant, flinty rocks, whereas diabasic breccias remain friable and unannealed

3. local melting of plagioclase grains as evidenced by spherulites that radiate into the breccia matrix (fig. 35).

The spherulites appear to have formed from melting along the edges of grains (fig. 35a, b), or may have originated from the center of a grain that entirely melted (fig. 35c). Once melted, the small volumes of liquid quenched, possibly because they combined with water in the sheared matrix to form the feathery spherulites. The association of this melt-texture with breccia zones suggests that the melting arose from frictional heating generated by the brecciation. If the

Breccia Textures

Fig. 34.--(a) sheared zones surrounding rounded domains of relict texture. Crossed polarizers, 1 in. = 3 mm.

(b) breccia matrix of sutured quartz + epidote + chlorite. Crossed polarizers, 1 in. = 3 mm.

(c) granulation and epidote-formation along plagioclase grain boundaries. Crossed polarizers, 1 in. = 0.4 mm.

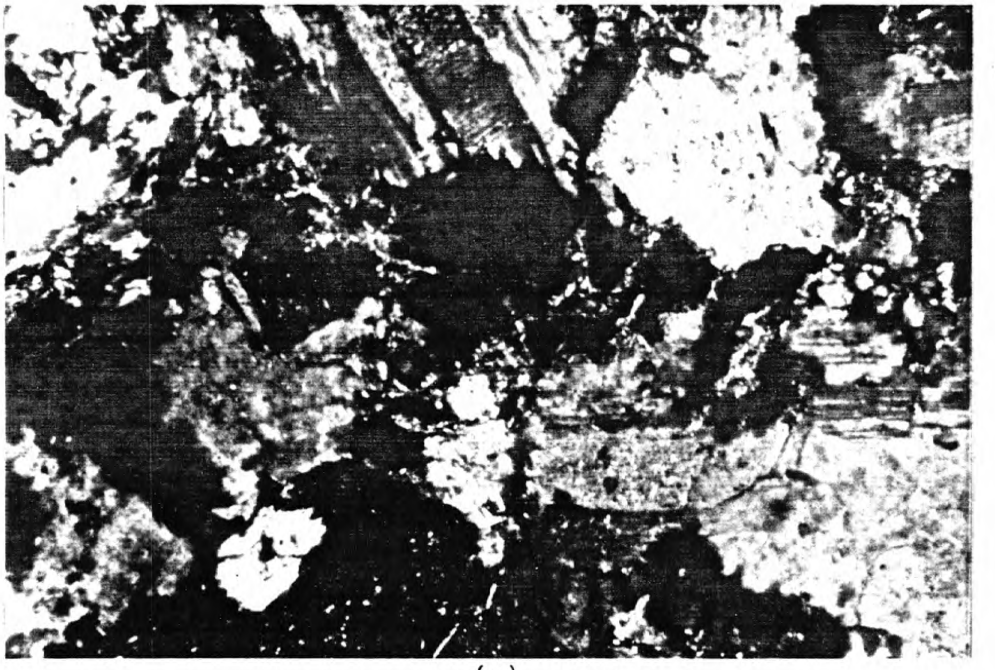

(a)

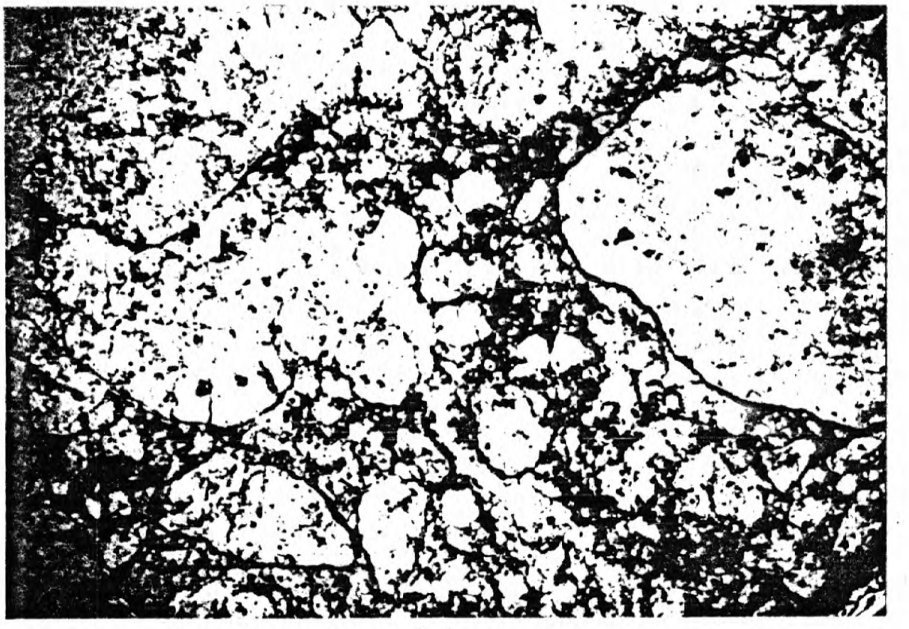

(b)

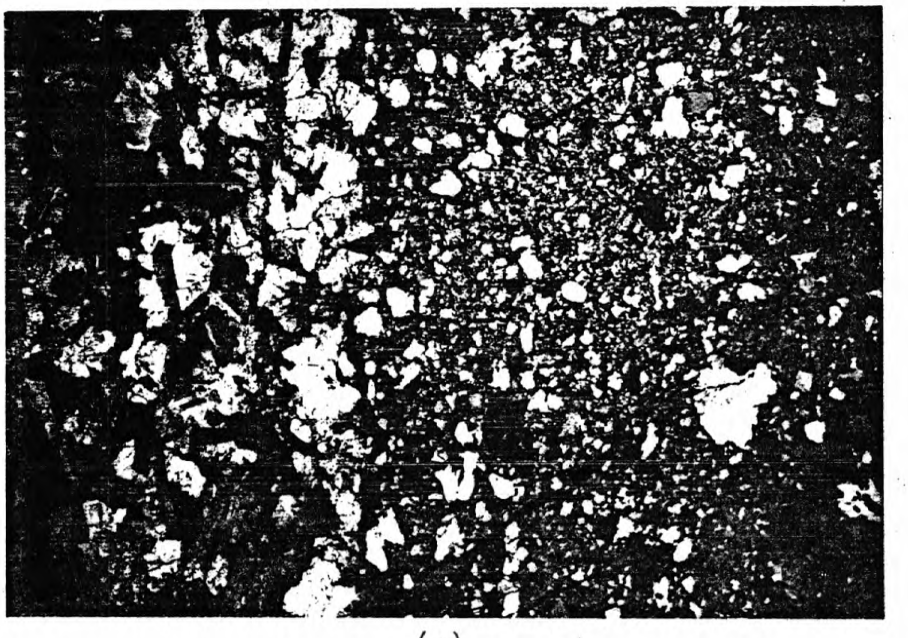

(c)

Melt-Textures in Brecciated Quartz-Albitite

Fig. 35.--(a) spherulites originating from the melted edges of a plagioclase grain, extending into breccia matrix. Crossed polarizers, 1 in. = 0.2 mm.

(b) detail of broken and melted grain in (a). 1 in. = 0.1 mm.

(c) spherulites originating at centers of entirely melted grains. 1 in. = 0.2 mm.

(a)

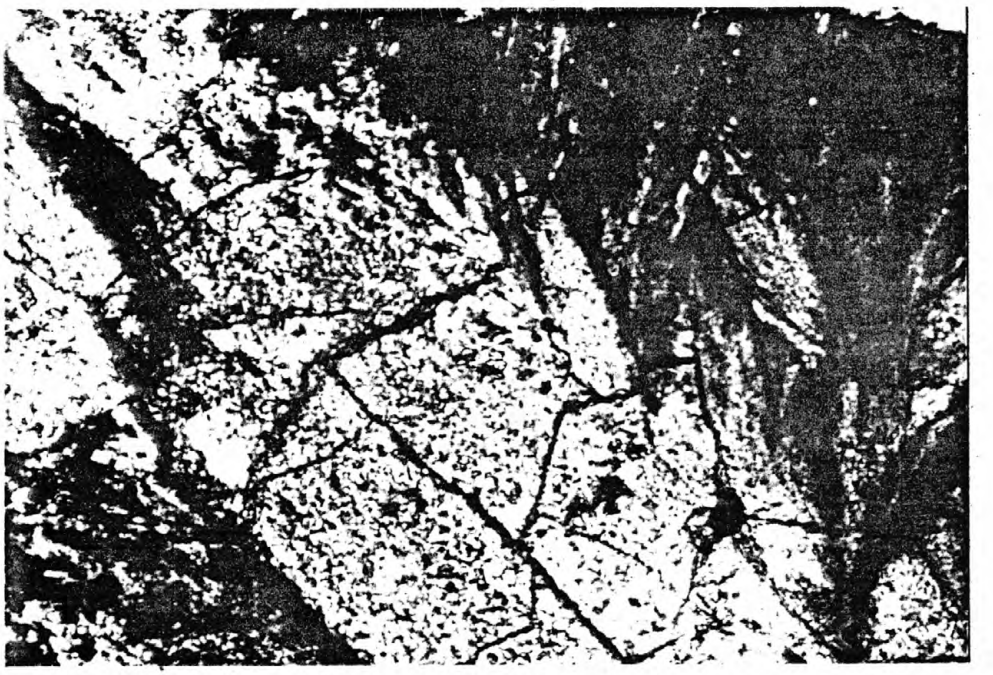

(b)

(c)

temperature of the rock was above 260°C but below 400°C at relatively low pressure (see below p. 144), then the frictional heating under shearing stresses could have created locally superheated spots within the rock. The local temperature would have been raised to the solidus of the microsystem at those spots. If the effective pressure created by shearing was 3 to 5 kb, the temperature would have needed to change by 300°C to 100°C to reach the (H_2O-saturated) granite liquidus (Turner and Verhoogen, 1960).

Breccia textures of this type are rare in terrestrial rocks. Similar textures do exist in rocks at Sudbury, Ontario, and at the Vredefort Dome, South Africa, as well as in lunar breccias (H. G. Wilshire, pers. comm.). A fine-grained glasslike rock, called pseudotachylite, from Sudbury and the Vredefort Dome, is a breccia formed from intense frictional heating (Wilshire, 1971). Although many features of the pseudotachylite differ significantly from characteristics of the Cuesta Ridge breccias, there are seven striking similarities:

1. The breccias are highly localized within portions of the rock masses in which they are found
2. The breccias have the same bulk composition as the rocks in which they occur
3. The textures comprise finely brecciated zones surrounding zones of relict rock-texture or of coarse metamorphic recrystallization
4. In felsic rocks the matrix is mostly epidote + chlorite + quartz
5. Spherulitic crystallization textures are common
6. The breccia matrix often contains unstrained microcrystalline quartz grains with complex, sutured boundaries
7. Melting phenomena are developed in brecciated felsic rocks.

The texture of several rocks from the Cuesta Ridge intrusive complex (fig. 36) bears a close resemblance to some pseudotachylites from Sudbury, Ontario. The Cuesta Ridge rocks initially appeared to be porphyry. Plagioclase "phenocrysts" in this sample (fig. 36a, b) are of quartz + albite + actinolite + opaques. The quartz is unstrained, and has sutured or polygonal boundaries. Under high magnification, boundaries between the plagioclase "phenocrysts" and the groundmass are irregular, as though they have been abraded. Boundaries within compound plagioclase "glomerophenocrysts" obviously are granulated (fig. 36). By comparison with pseudotachylite textures, the rock may be interpreted as a breccia which has recrystallized without melting.

Wilshire (1971) notes that association of pseudotachylites from Vredefort Dome with planar shock-metamorphosed features in feldspars and micas and with basal deformation lamellae in quartz. The crushed material was injected into fractures of unbrecciated rock and much mixing of different rock types occurred. Wilshire estimates that the pseudotachylite formed at transient pressures of over 35 kb. This material formed during a high-energy explosive event, possibly a volcanic eruption (Bischoff, 1962) or a meteorite impact (Wilshire, 1971). In contrast, the friction-melt breccias of the Cuesta Ridge felsic sills neither are associated with shock metamorphism, nor are injected into faults or fractures, nor are mixed or flowed. The brecciation appears to have been static, localized along intrusive contacts or in other areas of weakness, such as the interstitial areas of granophyric intergrowth, more like pseudotachylites studied in Silvretta by Masch (1973).

Breccia "Porphyry"

Fig. 36.--(a) matrix and residual faulted plagioclase megacrysts. Crossed polarizers, 3 mm long.

(b) detail of "phenocrysts" and matrix. Crossed polarizers, 1 in. = 0.4 mm.

(c) detail of large grain with crumbled borders in sutured-quartz + albite matrix. Crossed polarizers, 1 in. = 0.2 mm.

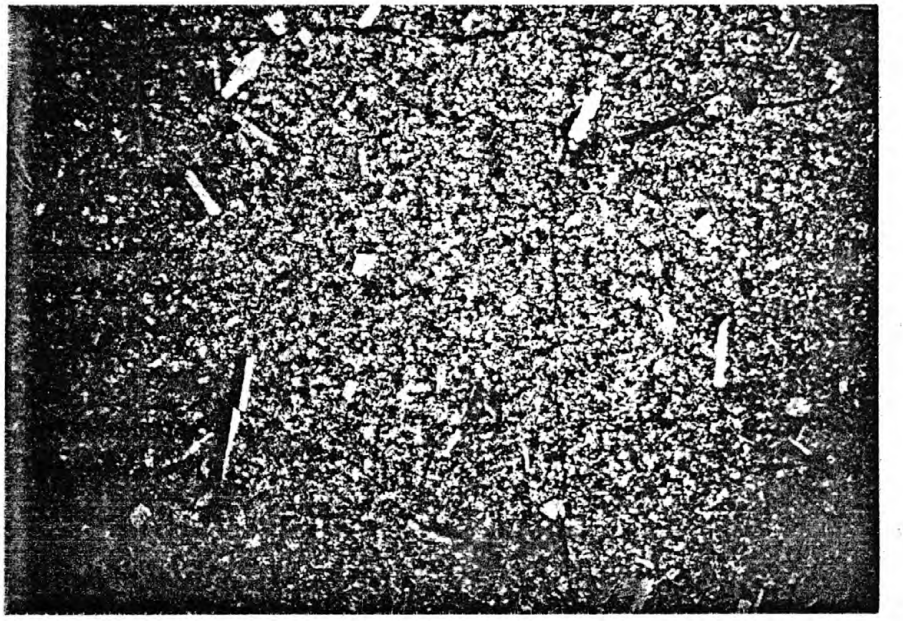

(a)

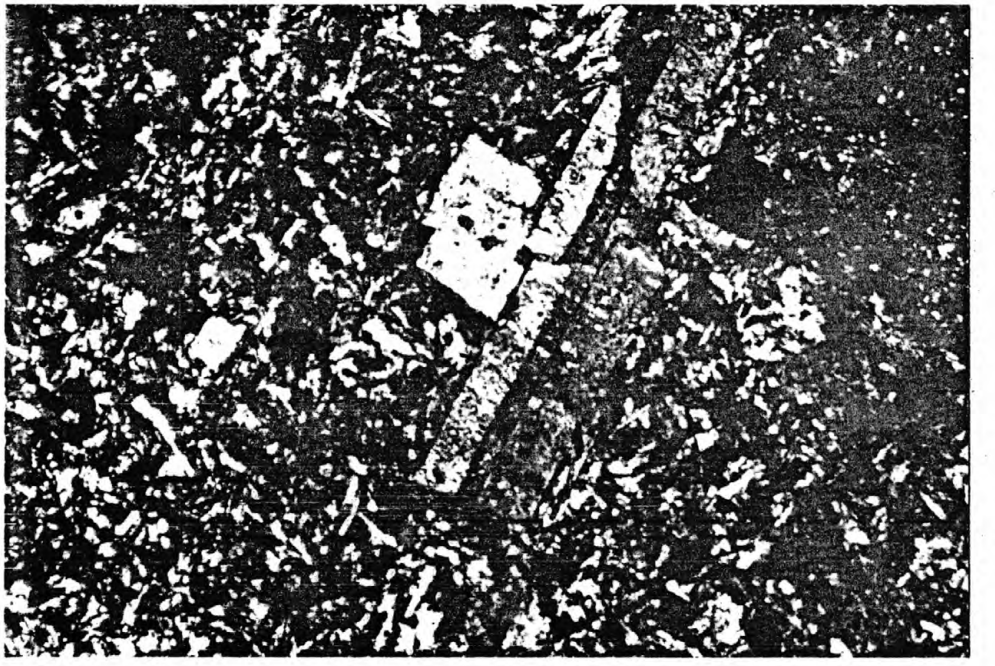

(b)

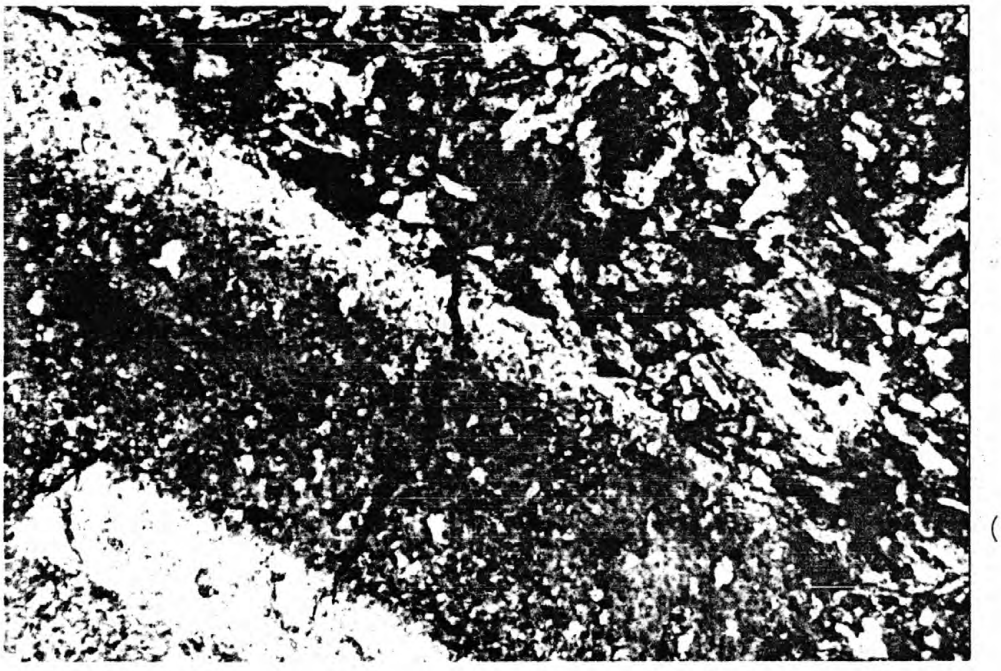

(c)

The annealing textures in the Cuesta Ridge breccias and their mineral associations indicate that brecciation occurred within the stability field of greenschist-facies. Because the rocks deformed in a brittle fashion they must have sheared at temperatures well below their solidi. Melting was localized on a scale of fractions of mm. At a few localities there is evidence of some plastic deformation of rocks prior to (or perhaps during) brecciation. Figure 37 illustrates one of the outcrops in the Cuesta Ridge complex where a diabasic dike that intruded quartz-albitite was deformed plastically (and later faulted). The dike and portions of the quartz albitite are brecciated.

The type of event or events that caused the localized shearing of rock is not evident from field observations in the intrusive complex. Because brecciation is associated with contacts and is discordant to the faults associated with emplacement of the ophiolite, the shearing must have taken place during initial formation of the ophiolite rather than during the subsequent events of emplacement.

Summary

The chemistries and textures of the intrusive complexes provide important clues to the formational history of the entire San Luis Obispo ophiolite body. The complexes are layered intrusive masses that resemble differentiated, stratiform-type mafic-ultramafic bodies. One of the complexes contains cumulate ultramafic and mafic rock, although the characteristic layering has been dismembered by tectonic disturbances subsequent to formation of the stratiform body. Such movements would include emplacement of the ophiolite as a thrust-like plate over Franciscan rocks.

Fig. 37.--Sketch and photograph of outcrop with folded dike in quartz-albitite.

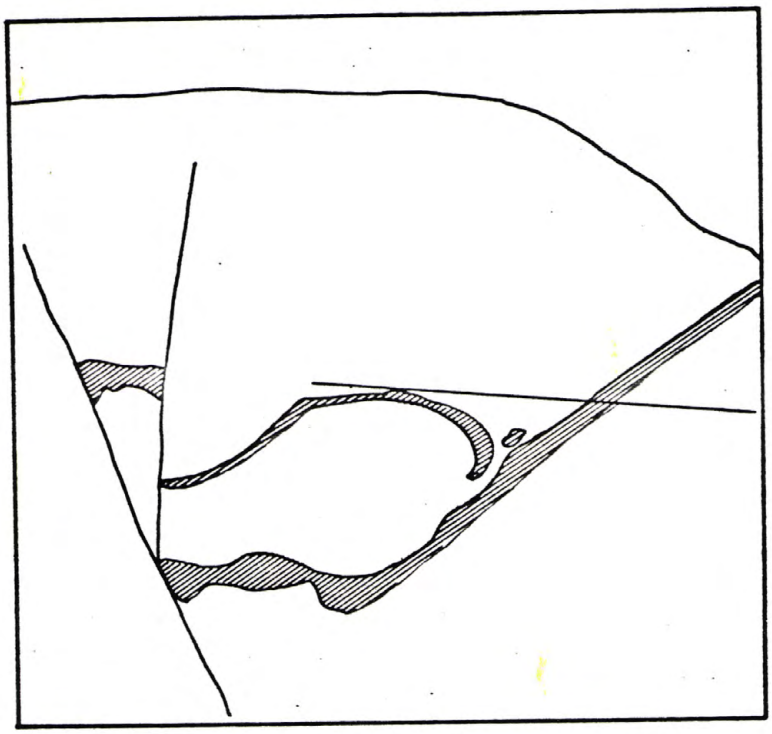

Fig. 37.--Plastic deformation in brecciated sills of the Cuesta Ridge intrusive complex.

The Cuesta Ridge intrusive complex clearly postdates formation of the ophiolite volcanic pile because felsic sills of the complex intrude the lavas. Intrusive relations among the sills show that formation of the complex was a multistage process: gabbros are intruded by quartz-diorite and both rocks are then intruded later by quartz-albitite and diabasic sills and by diabasic dikes. Multistage textures in the upper gabbro body suggest that partial melting of the cumulate gabbros has formed the later, more felsic intrusions. The early-formed garnet-bearing rocks, now retrograded to chlorite + albite, and hornblendes preserved in mafic rocks, imply a high-temperature metamorphic episode, perhaps related to the melting. A late stage of partial melting in the lower ultramafic sequence may be indicated by the late intrusion of diabases into the cumulate ultramafics and overlying quartzo-feldspathic rock sequence. Brecciation of the late sills and dikes suggests that intense but locally-concentrated stresses acted upon the rocks before they were cooled below about 300°C, prior to emplacement.

CHAPTER VI

CHEMISTRY AND ALTERATION OF THE SAN LUIS OBISPO OPHIOLITE

Chemistry, minerals and textures of rocks in the San Luis Obispo ophiolite provide a basis for reconstructing the conditions and events involved in its genesis. Basal ultramafic rocks may be parental to the basic dikes, mafic-ultramafic complexes, and basaltic lavas that intrude and overlie them. Subsequent melting events that affected portions of the stratiform gabbroic intrusions may have produced felsic liquids. The felsic liquids differentiated to become a sequence of quartz-diorite and quartz-albitite sills that intruded the stratiform complex.

The events that formed and metamorphosed the ophiolite occurred at both high and low temperatures. Conditions of high temperature in an unknown (but probably moderate--no more than 5 kb) pressure range prevailed in the early formational and metamorphic history of the complex. Relics of primary pyroxene and calcic plagioclase show that the mafic rocks crystallized at high temperature. Subsequent high-temperature metamorphism of the basic rocks in the presence of aqueous fluid produced hornblende in gabbros of the Cuesta Ridge intrusive complex and amphibolites of the Cerro Alto intrusives. Later retrogressive metamorphism of the entire ophiolite suite occurred as the result of a marked drop in the temperature of the environment, although the pressure appears to have remained in the

vicinity of 5 kb (and may have been as low as 3 kb). The drop in temperature coincided with a change in the tectonic environment from relatively stable conditions, under which a stratiform cumulate complex developed, to conditions of instability, in which felsic and diabasic rocks were locally brecciated and felsic rocks were partially melted. The conditions of tectonic instability probably arose at the onset of subduction of the crustal plate containing the ophiolite. Explosive volcanism and localized failure of rocks under high strains may have precipitated the shocks that caused brecciation.

Chemical Relations Among Rocks of the San Luis Obispo Ophiolite

The formation of igneous rocks in the San Luis Obispo ophiolite appears to have required several stages. The first stage was the introduction of parental mantle peridotite (which may or may not still be present in the ophiolite ultramafic rocks) into an area of exceptionally high heat flow, where resulting thermal instabilities induced melting and generated basaltic magmas. The heat input needed to produce melting in mantle rocks is so great, whether wet or dry, that an environment of high thermal gradient is required. Temperatures of melting in anhydrous peridotite at atmospheric pressure approach 1200°C (O'Hara, 1967a) in natural four-phase lherzolite and are much higher in three-, two- or one-phase ultramafic rocks. The melting temperatures for all the dry ultramafic rocks also increase with increasing pressure (O'Hara, 1967a). These temperatures may be lowered considerably by introducing volatiles, to about 1000°C if the system is water-saturated (an unlikely possibility).

The second stage of ophiolite genesis was the formation of a stratiform cumulate body, probably from fractionation of basaltic magma. This stage also occurred at high temperature. The chemistry of all the ophiolite rock types defines well-marked fractionation trends on a Harker diagram (fig. 38). Such trends suggest that either (1) the entire ophiolite rock association formed from the fractionation of a single basaltic (gabbroic) melt that produced crystal residue of ultramafic rocks and gabbros plus felsic liquids, or (2) a series of basaltic partial melts produced the gabbroic rocks and basaltic lavas after very little fractionation, but some of the melts underwent extensive fractionation to produce ultramafic and gabbroic cumulate rocks and felsic liquids.

Field and textural evidence within the ophiolite rocks indicates that the second interpretation is the more likely, and that the history of the ophiolite probably is even more complex than this alternative implies. Field relations indicate that the lavas were erupted prior to intrusion of the stratiform cumulate complex, and that the cumulate complex was itself intruded by diabases late in the igneous genesis of this ophiolite. According to the evidence, several basaltic melts were generated rather than one stage of melting and fractionation that produced all the rocks of the ophiolite. The multistage gabbro textures (Supra p. 86) indicate further that the third stage of ophiolite formation was partial melting of some of the gabbros. Chemical compositions in the intrusive complex indicate that this melting could have produced the felsic sills.

Field evidence supports the production of felsic sills from melting of gabbros. The dioritic and quartz-albitite sills in the

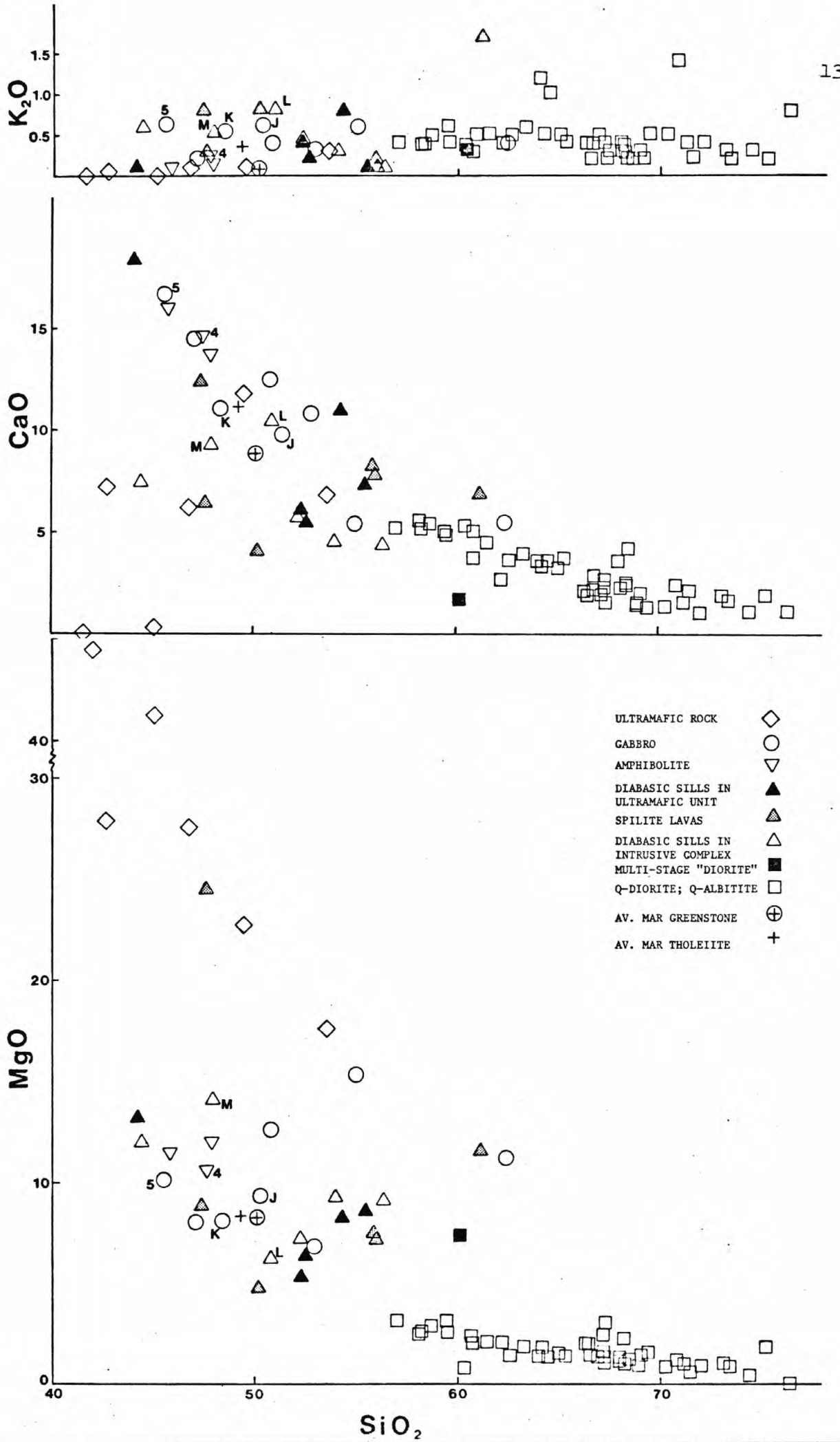
K2O
1.5
1.0
0.5
CaO
15
10
5
MgO
40
30
20
10
0
40
50
60
70
SiO2
ULTRAMAFIC ROCK
GABBRO
AMPHIBOLITE
DIABASIC SILLS IN ULTRAMAFIC UNIT
SPILITE LAVAS
DIABASIC SILLS IN INTRUSIVE COMPLEX
MULTI-STAGE "DIORITE"
Q-DIORITE; Q-ALBITITE
AV. MAR GREENSTONE
AV. MAR THOLEIITE

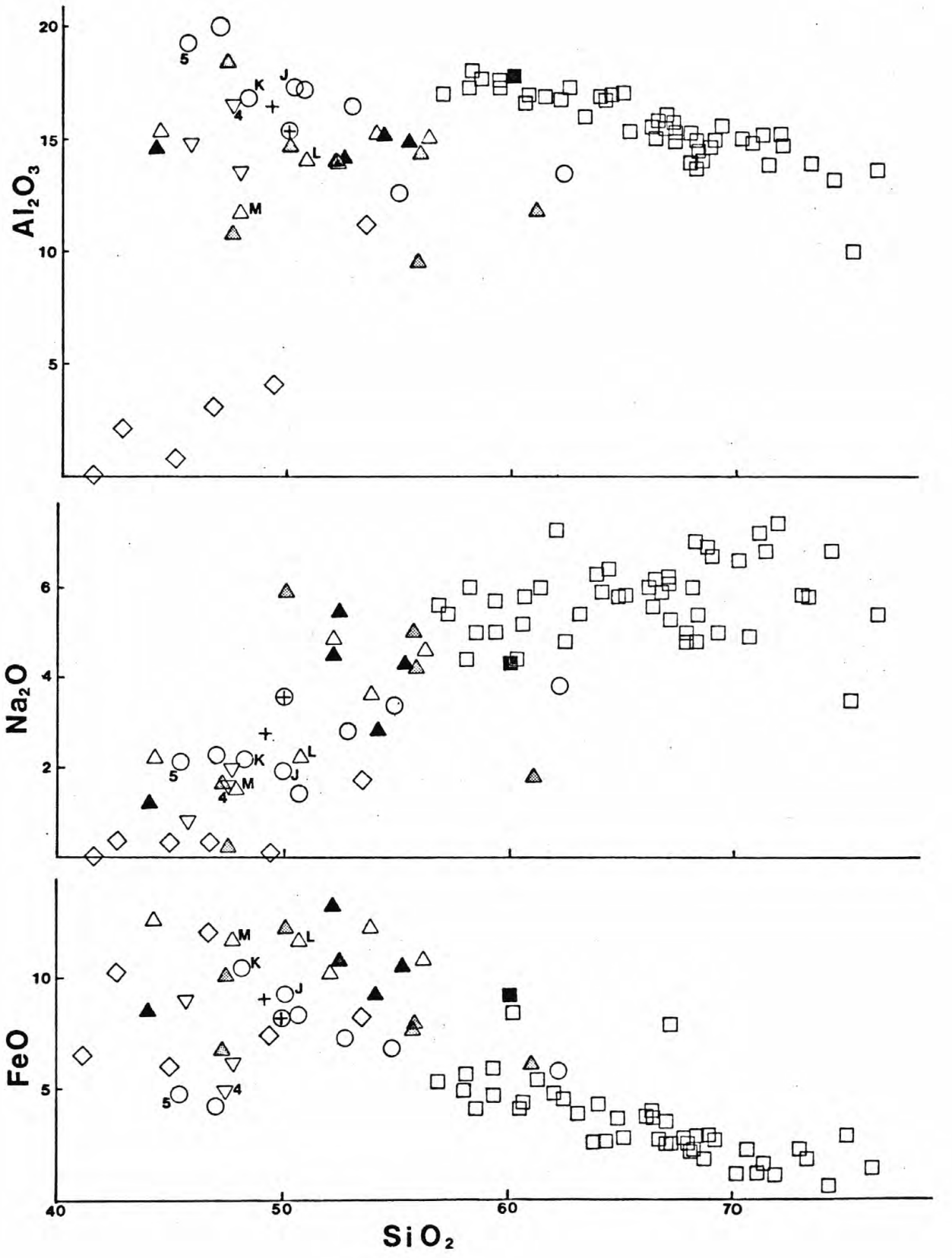
20
15
10
5
Al_2O_3
5
J
K
4
L
M
6
4
2
Na_2O
5
K
L
J
M
4
10
5
FeO
M
L
K
J
5
4
40
50
60
70
SiO_2

Cuesta Ridge complex intrude gabbros at the base and top of the intrusive sequence, indicating that the sills formed after consolidation of the gabbros. The complex contains very little gabbro relative to felsic rock, which is opposite to the relative abundances of these rock types in other ophiolites (Pt. Sal, California, Hopson and Frano, 1973; Canyon Mountain, Oregon, Thayer and Himmelberg, 1968; Troodos, Cyprus, Moores and Vine, 1971). This difference indicates that (1) gabbroic portions of the cumulate sequence were lost by faulting, and/or (2) some gabbroic layers were removed by being melted and differentiated to produce the felsic sills.

Whether or not melting gabbros would produce the felsic rocks of the Cuesta Ridge complex was tested, using chemical compositions of rocks and minerals found in the sill sequence. In figure 39 the Harker diagrams for FeO, CaO, Na_2O and K_2O have been reduced to outline fields of rock-compositional ranges and points marking compositions of possible parent melts and products. It was assumed that melting would have generated a composition similar to that of gabbro 12 (table 11), which is similar to a melt produced from a tholeiitic basalt composition at low pressure (O'Hara, 1965) (except that MgO is too high, so it was not plotted). The melt composition is plotted as a square in figure 39. The compositional range of ultramafic rocks is outlined with dots, gabbro and diabase by dashes and felsic rocks by alternating dots and dashes. The arrows show trends of residual crystals (R) and liquids (L) produced from fractional crystallization of 20 percent pyroxene and 50 percent plagioclase from 20 percent crystallization of the melt. The mineral compositions are those of analyzed pyroxene (Appendix Ia-C) and intermediate-zone

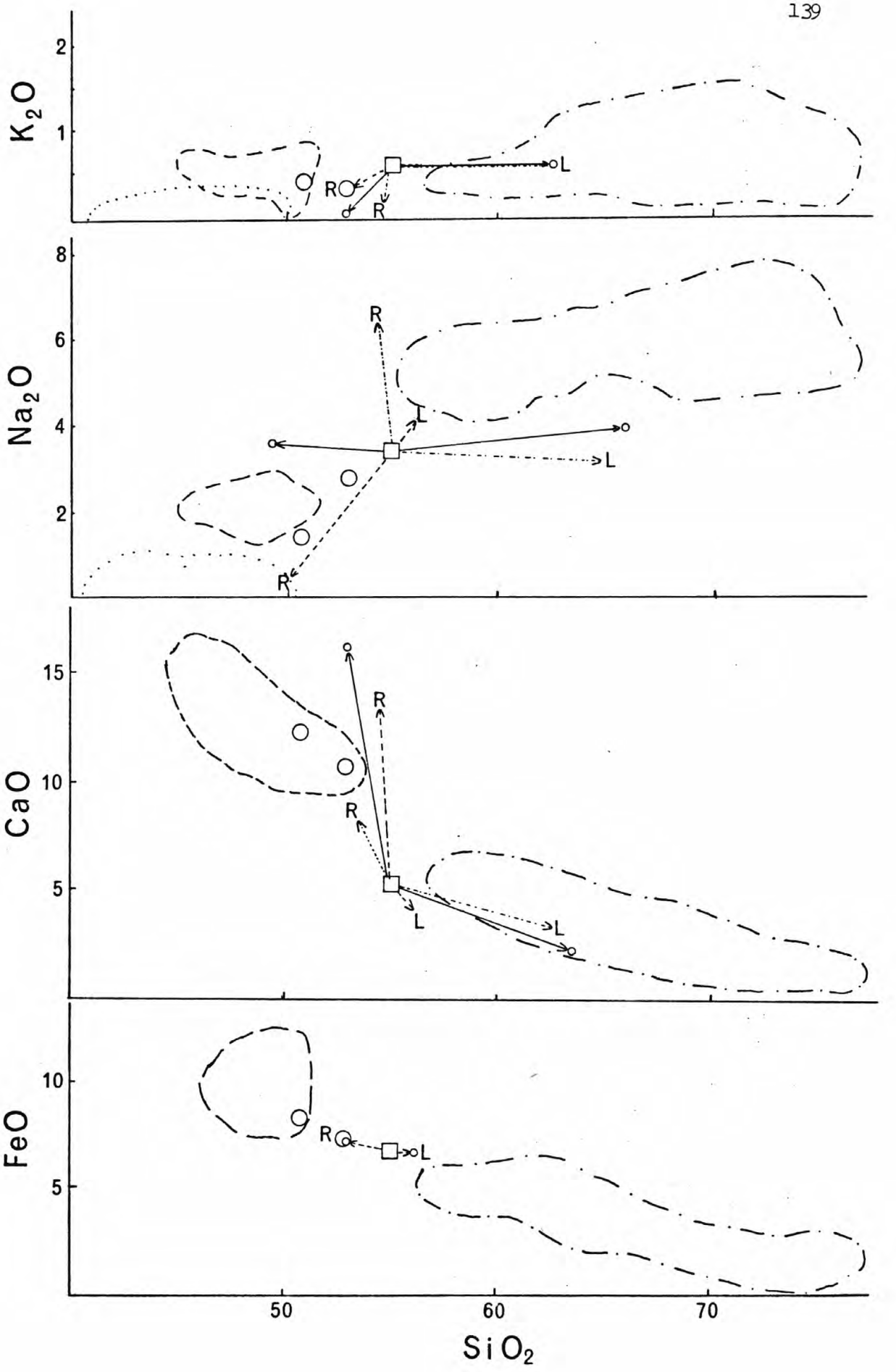
K2O
2
1
R
R
L
Na2O
8
6
4
2
R
L
L
R
CaO
15
10
5
R
R
L
L
FeO
10
5
R
L
50
60
70
SiO2

plagioclase (A, table 13) from the multistage gabbro (14, table 11). According to figure 39, this mechanism for generating the felsic rocks is feasible, although not necessarily verified by the calculations. However, the textures, intrusive relations, and chemical relations strongly suggest that melting within the gabbroic rocks produced the later felsic liquids. These liquids must have differentiated further to produce the chemical stratigraphy of increasing SiO_2 and decreasing CaO contents from base to top of the sill complex (Supra, figs. 25, 28).

The fourth stage of ophiolite genesis was renewed melting in the mantle to produce late diabases of the intrusive complex. Field relations suggest that the diabases may have been the very last rocks to intrude the sill complex, and that they may have been late feeders for the overlying volcanic pile. The very similar basalt and diabase compositions shown in figure 38 support this inference.

According to Blake and Bailey (1973), chemical trends in the San Luis Obispo and other California ophiolites strongly indicate that the mafic rocks were derived from the associated sheared ultramafic rocks, which represent the mantle. However, Sr^{87}/Sr^{86} determinations in ultramafic rocks and associated basaltic lavas from Red Mountain, California, and Canyon Mountain, Oregon (Lanphere, 1973), indicate that the rock types cannot have a direct parent-daughter chemical relation. Similar studies on the San Luis Obispo ophiolite are required to determine if the same problem exists in this mafic-ultramafic rock association.

Effects of Metamorphism on Ophiolite Chemistry

The rocks in this ophiolite have undergone two discernible metamorphic episodes: an early one at high temperature and a later one at low temperature. Although the high temperature event is obscured by the low-temperature metamorphism, enough mineral relics survive to indicate the possible conditions involved in the earlier event. Some of the amphibolite was little changed in the low-temperature event. The mineral composition of these rocks indicates that the high-temperature metamorphism occurred at almandine-amphibolite facies temperatures, although there is no good indication of the pressures involved. Compositions of hornblendes and plagioclase (Appendix Ib, c) indicate that the temperatures could not have been greater than 800°C without the appearance of pargasitic amphiboles.

The first metamorphic episode resulted from hydration of the mafic rocks at high temperature. Whole-rock compositions of the amphibolites (fig. 38) indicate that the rocks were not appreciably changed from their probable olivine-gabbro primary compositions. Felsic sills do not contain any evidence of this high-temperature metamorphism and so the episode may have occurred before formation of quartz-diorite and albitite.

All the rocks of the San Luis Obispo ophiolite have been retrogressively metamorphosed in the pressure-temperature range of the greenschist facies. The major effects of alteration are similar in all the mafic and felsic rocks: Ca has been leached, while SiO_2 and Na_2O have been added. The source of added SiO_2 and Na_2O is unknown at the present time. Although Na_2O could be added from sea water

to the spilite lavas this cannot be true for SiO_2 in the lavas or for SiO_2 and Na_2O in the intrusive rocks. Melson and Van Andel (1966) speculated that juvenile fluids must cause Na- and Si-metasomatism in the oceanic crust, and this is possible, although unproved. The resulting mineralogy is actinolite + epidote + quartz + chlorite. In some reacted rocks MgO has been leached from the centers of rock bodies (pillow cores, centers of diabasic intrusions) and concentrated in the rims.

Serpentinization reactions also appear to promote the mobility of Ca by leaching orthopyroxenes. Several of the plots in figure 38 show evidence of rock alteration. The primary result of alteration is the high SiO_2 contents of the diabasic and basaltic rocks and several of the gabbros. Comparison with fresh basalt compositions plotted on the same diagrams (5, 6; 16, 17; 22, 21; and cross) demonstrates that normal mafic rocks contain 45 to 51 percent SiO_2, whereas the San Luis Obispo ophiolite diabases and gabbros tend to contain 50 to 57 percent SiO_2. The diabases also tend to have high Na_2O (3 to 6 percent) and low CaO (5 to 7 percent). However, all of the amphibolites and three of the gabbros retain their high-Ca and low-Si contents and hence reflect the primary compositions.

Alteration also is evident in the CaO and MgO distributions of figure 38. There are two branches to each of these plots at low SiO_2 values. The low-Ca branch of the CaO-SiO_2 plot represents serpentinized ultramafic rocks that normally are low in CaO, but that also have lost CaO through serpentinization reactions. The other rocks in the low-Ca trend are diabases, whose low CaO contents are due to alteration. Similarly, the most Ca-rich point in the high-CaO trend

is the rodingitized border of a diabase (G, table 1), a composition also influenced by alteration. Minor MgO enrichment in a pillow rim is evident in the MgO-SiO_2 plot; a lava composition that falls along the ultramafic trend is the MgO-rich rim of a pillow. In general, spilitization and greenschist alteration have not radically changed the MgO or total iron contents of these rocks, as indicated by the plots of fresh rock compositions (fig. 38; tables 5, 10, 14). Comparison of the compositions of average Mid-Atlantic Ridge tholeiites and greenstones in figure 38 indicates that MgO probably changes the least in greenschist alteration. Although there is local movement of MgO within the pillows, most of the MgO enrichment resulted from leaching away of other elements, notably aluminum and calcium.

Trace element data from San Luis Obispo lavas (Supra p. 64) indicate that the basaltic rocks were tholeiitic before alteration; the low K_2O contents substantiate the inference. The K_2O contents of all the San Luis Obispo ophiolite rocks are quite similar and only exceed 0.8 percent for 5 of the 73 rocks analyzed. K_2O forms no primary phase in any of the rocks, and does not appear to have been leached from the rocks in large amounts, because no K-rich vein fillings or alteration zones occur in the exposed rocks. Accordingly, the low K_2O contents are characteristic of this rock association and imply that all rocks in the ophiolite are derived from a low-K source.

Conditions of Greenschist Facies Metamorphism

Greenschist-facies metamorphism affected all rocks of the San Luis Obispo ophiolite before they were finally emplaced into a

continental margin at the Earth's surface. The conditions of this metamorphic event which differed distinctly from the early formational conditions of the assemblage, coincided with the onset of tectonic disturbances that probably occurred during oceanic plate subduction.

Experimental work on greenschist-facies minerals indicates that the low-temperature limit of the paragenesis is defined by the actinolite compositions and the presence or absence of pumpellyite in the assemblage. The minerals albite ± actinolite + chlorite + epidote + quartz are present in all the mafic and felsic rocks of the ophiolite. Prehnite joins the assemblage only in the diabases and amphibolites that intrude serpentinites. Nitsch (1971) demonstrated that pumpellyite should occur in the assemblage of basic rocks metamorphosed at temperatures below 345°C at 2 kb and 260°C at 7 kb (fig. 42). Absence of pumpellyite in the San Luis Obispo rocks indicates that the metamorphism occurred at temperatures above those of pumpellyite stability, in the field marked "greenschist" in figure 40.

The presence and amount of tetrahedrally-coordinated aluminum in amphibole is a sensitive indicator of metamorphic grade in basic rocks (Ernst, 1968). The reaction tremolite = diopside + enstatite + quartz + fluid occurs at temperatures of 725 to 900°C under fluid pressures of 250 to 3000 bars (Boyd, 1959). Pargasite, which contains the maximum number of Al atoms that can substitute in Ca-amphiboles, breaks down at basalt liquidus temperatures (800 to 1050°C) under fluid pressure of 200 to 1500 bars (Boyd, 1959). Addition of Fe to either tremolite or pargasite considerably lowers the stability limit, for ferrotremolite it is lowered to 400 to 500°C (Ernst, 1966;

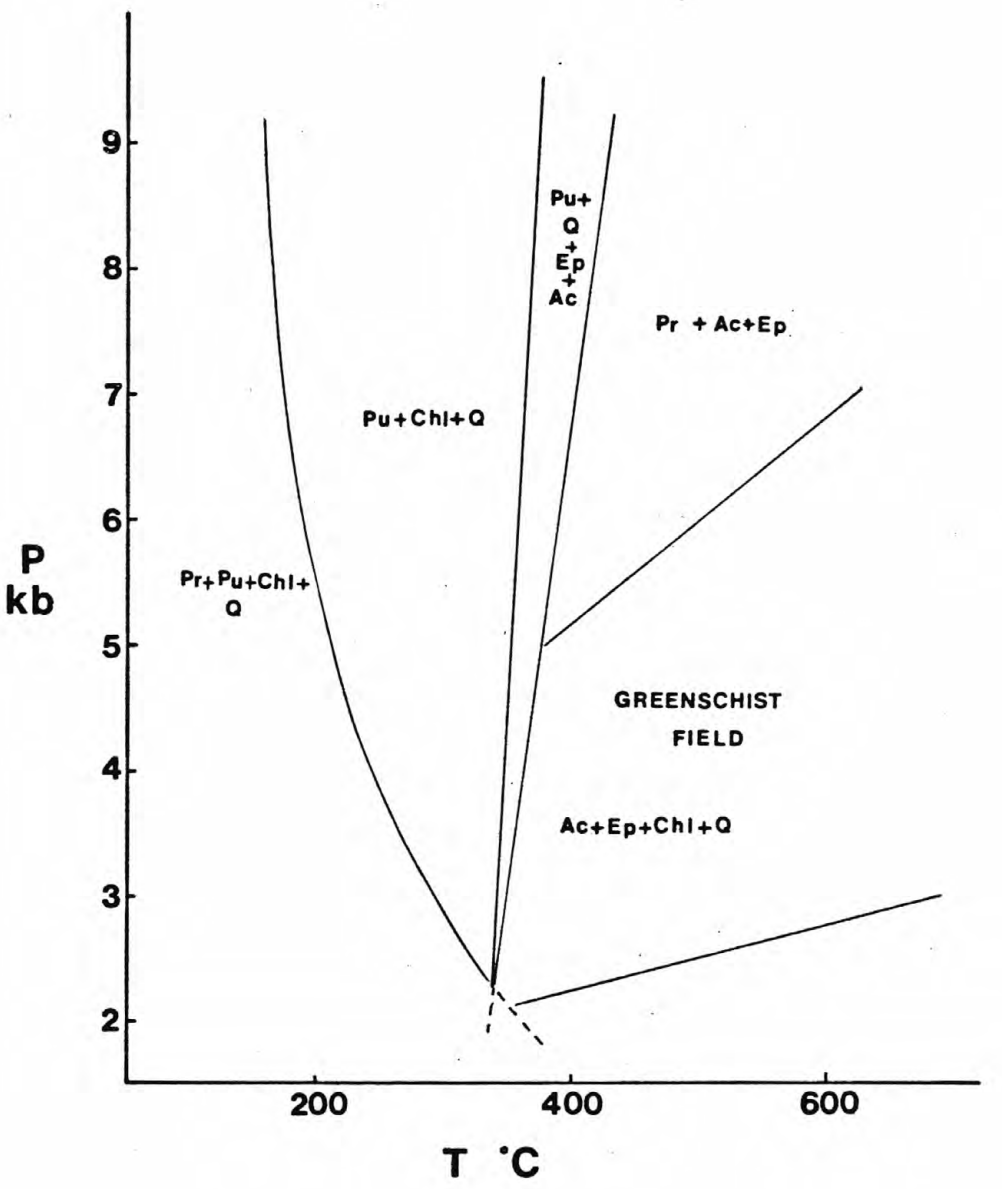
P
kb
9
8
7
6
5
4
3
2
200
400
600
T °C
Pu+
Q
+
Ep
+
Ac
Pr + Ac+Ep
Pu+Chl+Q
Pr+Pu+Chl+
Q
GREENSCHIST
FIELD
Ac+Ep+Chl+Q

fig. 41). Compositions of the San Luis Obispo tremolites and actinolites all fall between tremolite and pargasite in Al^{IV} content and all have Mg/Mg+Fe ratios of 0.6 or more (figs. 8, 17, 21, 32). Accordingly the presence of these amphibole compositions indicates metamorphic temperatures below 400 to 500°C at pressures between 300 and 3000 bars for the greenschist-facies alteration of San Luis Obispo rocks.

Epidote compositions do not supply any further clues to the alteration conditions because the stability fields still are largely undetermined. Work to date (Holdaway, 1972; Liou, 1973; Hoerman and Raith, 1973) reveals that epidote compositions depend on bulk composition of the rock, the fugacity of O_2 in the system, and the presence or absence of excess SiO_2 (Holdaway, 1972). These data indicate that the stability of stoichiometric epidote with respect to clinozoisite lies in a field with upper boundary of 600 to 725°C at 1 to 4 kb fluid pressure (fig. 42). The actual formational conditions depend on the availability of Fe in the reacting system and vary with the bulk composition. All of the greenschist mineral compositions point to metamorphic conditions of temperatures in the range 300 to 500°C at pressures that are not well-defined but may range from 3 to 5 kb (Nitsch, 1971).

Incipient melting in the brecciated felsic rocks indicates that the temperatures of greenschist metamorphism may have been as high as 400°C. Epidote formed abundantly in the breccia matrix, which is indicative of temperatures above 500°C for systems with high oxygen fugacity (Holdaway, 1972). Melting appears due to spots of frictional heating which locally raised temperatures higher than the albite-quartz

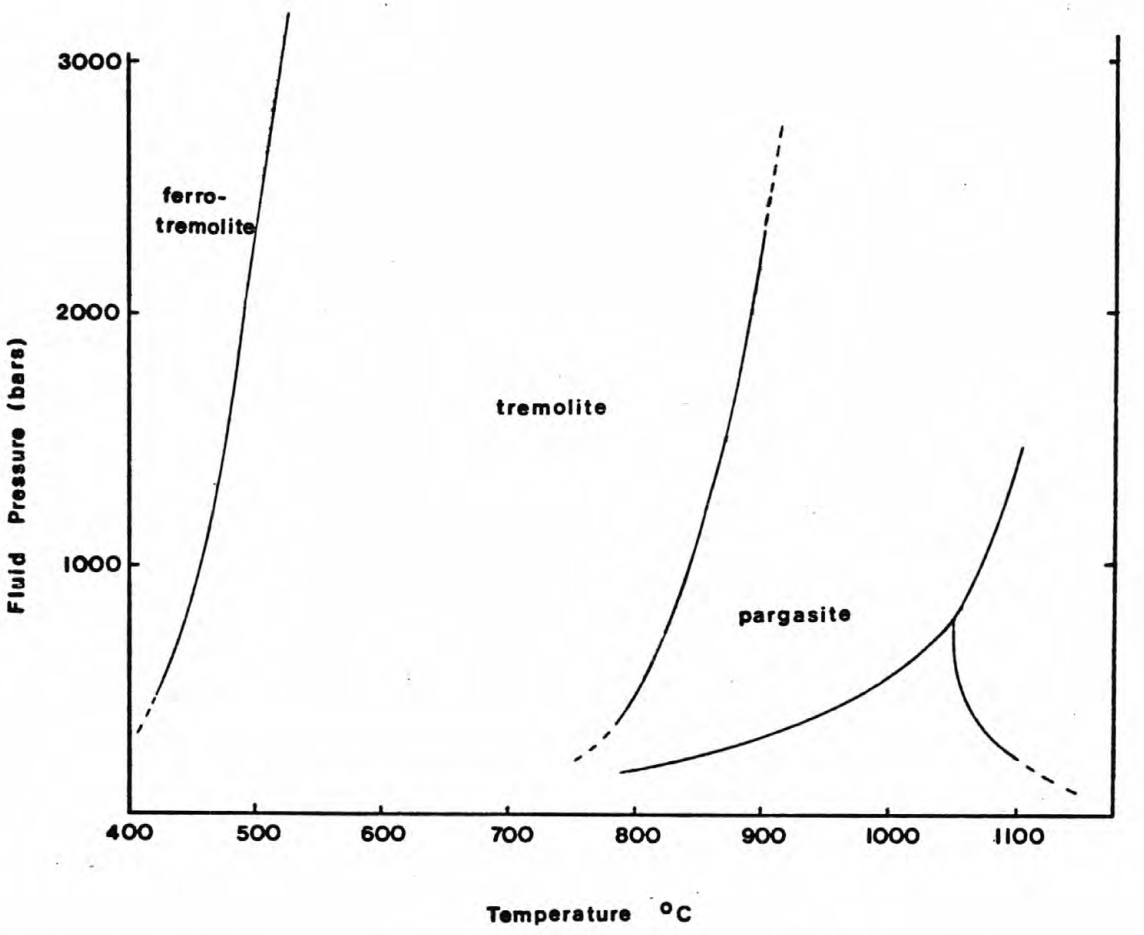

Fig. 41.--Stability limits of Ca-Mg amphiboles (Boyd, 1959; Ernst, 1966; Ernst, 1968).

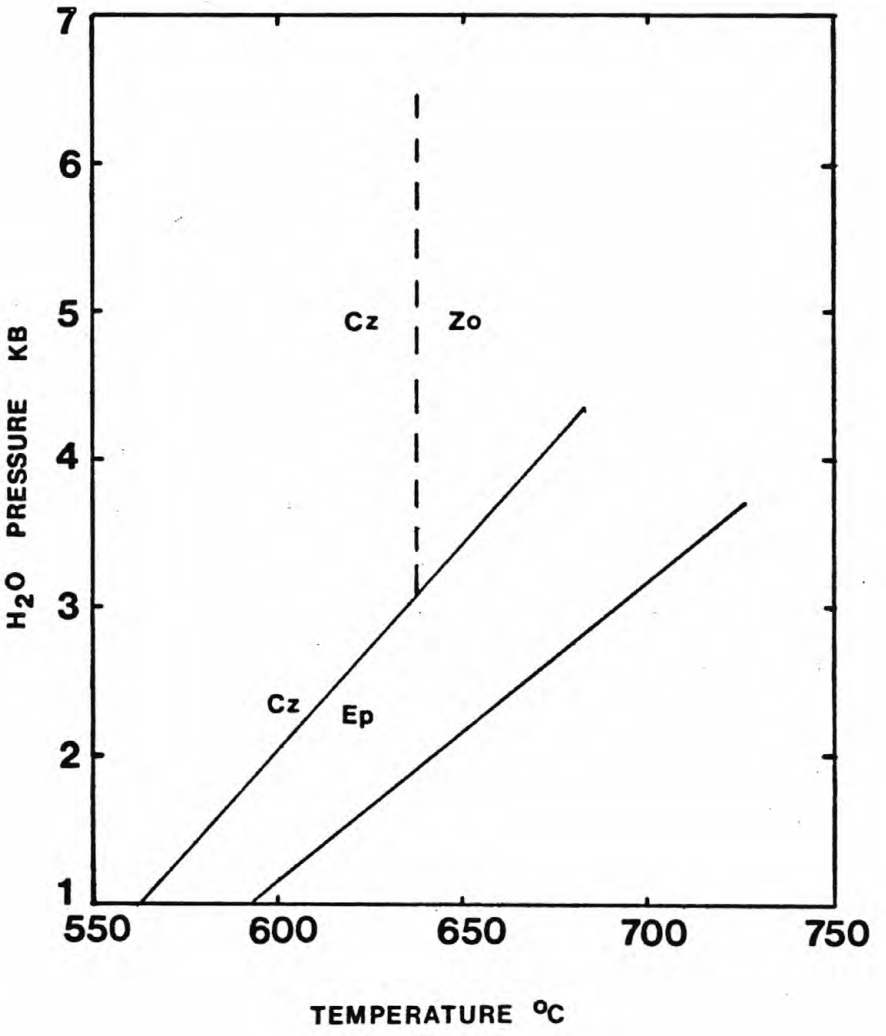

Fig. 42.--Stability limits of epidotes (from Holdaway, 1972).

Zo - zoisite
Cz - clinozoisite
Ep - epidote

solidus (about 600°C for H_2O-saturated conditions in the pressure range 3 to 5 kb, Turner and Verhoogen, 1960). Temperatures remained over 300°C following brecciation and allowed quartz to anneal any strain lamellae that developed during shearing (Griggs, et al., 1960).

It is unclear whether or not ultramafic rocks were altered (serpentinized) in the same environment as the mafic and felsic rocks. Although serpentine stabilizes relative to olivine at 500°C, there is evidence that much serpentinization occurs at very low temperature and at near-atmospheric pressures (Barnes and O'Neill, 1969). If these conditions apply to the San Luis Obispo ophiolite serpentinites, then the serpentinization did not occur at the same time as greenschist-facies metamorphism in the mafic and felsic rocks.

Summary

The San Luis Obispo ophiolite must have formed in an area of high temperatures, where tholeiitic magma was produced by partial melting of mantle material (possibly distinct from the ultramafic rocks present in the ophiolite). Some of the melt was extruded as lavas in a submarine environment, and some crystallized at depth as a stratiform cumulate complex. The complex was partly metamorphosed at high temperature by hydration, producing hornblende from the primary pyroxenes. Later, some of the cumulate gabbros may have been melted; these melts may have differentiated and been intruded as felsic sills into the remaining gabbros and into the lower portions of the volcanic pile. The last igneous stage in formation of the ophiolite was resumption of melting. This late event formed diabasic melts that were intruded into the sill complex and may have contributed more

lavas to the volcanic pile. The final stage of ophiolite formation occurred in cooler rocks, as the solid rocks were altered and brecciated at temperatures of 400°C or less and pressures that may have been between 3 and 5 kb. Transient heating during brecciation allowed incipient melting and subsequent annealing in the felsic rocks. The ultramafic rocks also may have begun to undergo serpentinization at this stage, but most of the serpentinization probably occurred after tectonic emplacement of the ophiolite into its present location.

CHAPTER VII

CONCLUSIONS

Chemistry, mineralogy and rock textures of the San Luis Obispo ophiolite suite support the hypothesis that an ophiolite sequence is a fragment of oceanic crust and mantle. The Ti-Zr data and the low-K tholeiitic nature of the basaltic, gabbroic and diabasic rocks indicate that the ultramafic-mafic sequence formed either at an oceanic ridge or an island arc. Textures and field relationships of the ophiolite intrusive rocks suggest that the early history of the complex was one of sporadic basaltic intrusion and extrusion. Long quiescent periods evidently allowed a stratiform cumulate complex to crystallize. An island arc environment, which is characterized by intense tectonism, does not correspond to the conditions in which the San Luis Obispo ophiolite formed. An oceanic ridge environment, especially if spreading is slow or stagnant, is a more likely site of formation for this rock association.

The absence of a sheeted dike complex suggests that the ophiolite could not have formed under the crest of an actively-spreading ridge. Instead, the ophiolite and its sill complex may have crystallized near the ridge flank, where temperatures may be high enough to melt peridotite mantle, under the correct conditions, but where igneous activity is less frequent. Whenever hydrous fluids were present in

these lower crustal areas high-temperature metamorphism of pyroxenes to amphiboles occurred.

The later low-temperature metamorphism and intensified tectonic activity may relate to the inception of rapid spreading at the ridge. The ophiolite would then have been transported, as part of the crustal plate, into an active arc environment and away from the high-heat ridge location. As the plate moved, the rocks contained in it became retrogressively metamorphosed. In the arc locale, earthquake and volcanic activity could have provided the transient stresses that brecciated the sills.

Model of Ophiolite Formation

Five stages of formation are apparent in the San Luis Obispo ophiolite (fig. 43):

1. Melting in peridotitic oceanic mantle produced basic lavas that intruded rocks of the lower oceanic crust and erupted into a submarine environment. Abundant vesiculation in the lavas indicates that the lavas were extruded in water no deeper than 2000 m (Moore, 1965).

2. The main mass of basic liquids may have formed a rising diapir (Green and Ringwood, 1967b) that expanded to become a crystallization chamber. A stratiform cumulate complex of ultramafic rocks and gabbros crystallized in this chamber, under conditions that remained quiet for a considerable time.

3. Intersection of the chamber with water-bearing portions of the lower crust may have caused melting in parts of the quartz-rich gabbroic cumulate rocks and high-temperature hydrous metamorphism

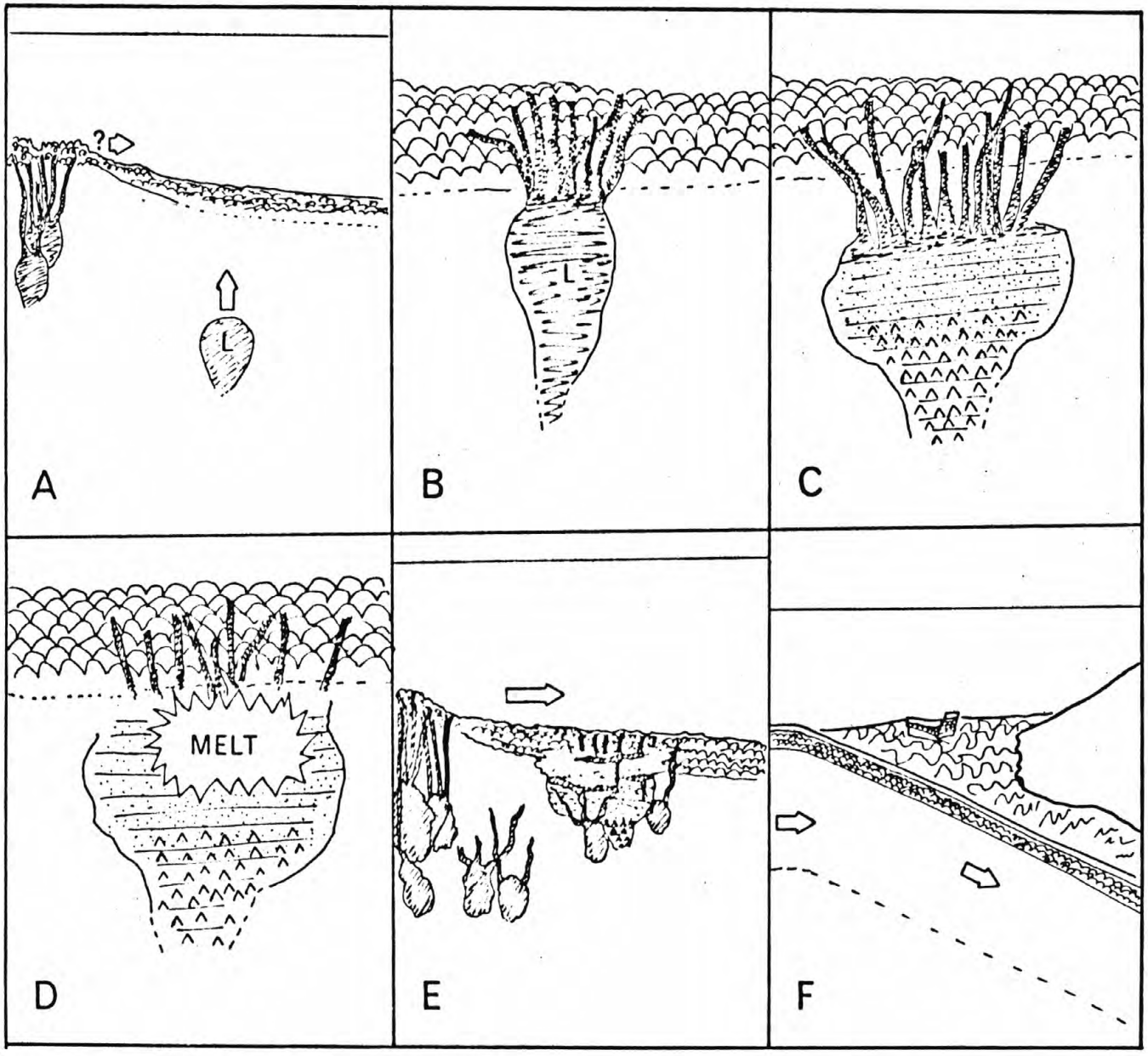

Fig. 43.--Stages in formation of the San Luis Obispo ophiolite.

of olivine gabbros to hornblende gabbro and amphibolite. Melting in the gabbros created felsic liquids that differentiated to form a sequence of sills. These sills intruded both the parent gabbros and the basalt lavas of the volcanic pile.

4. Late melting in the ultramafic mantle produced diabasic dikes that intruded the entire cumulate-and-felsic sill sequence and probably contributed more basaltic rock to the volcanic pile.

5. Following the high-temperature formational events, spreading of the oceanic plate may have begun or substantially accelerated, carrying the ophiolite rocks toward a colliding plate intersection. The ophiolite was transported away from the high heat flow area and began to be retrogressively metamorphosed at lower temperatures. After basaltic lavas were no longer extruded, sediments accumulated, burying the volcanic rocks to a depth of at least 700 m (Page, 1972). This sedimentary section formed during late Jurassic (Tithonian) to early Cretaceous (Valanginian). If the felsic sills formed at about 150 m.y. BP (Hopson, pers. comm.), the volcanism must have ended soon after. The emplacement of ophiolite into the continental margin probably occurred about 120 to 150 m.y. BP (Page, 1972). Thus, the greenschist metamorphism must have occupied a period of no more than 30 to 50 m.y. This time apparently was not sufficient for the low-temperature reactions to reach equilibrium before the oceanic plate was broken up by subduction and emplaced piecemeal over the subduction mélange. In the rocks studied there are no mineralogic relations indicating retrogression from high-pressure metamorphism, such as are characteristic of many Franciscan rocks. It is therefore probable that this ophiolite slab was never subducted.

In summary, relationships in the San Luis Obispo ophiolite suggest that it formed at a mid-ocean ridge, where conditions of high heat flow are usual. Pressures of formation are not well-defined, but imply a range of 3 to 5 kb throughout the oceanic history of the suite. These conditions place genesis of the ophiolite at depths between 5 and 10 km--the oceanic crust and mantle interface. The later metamorphism of the ophiolite retrograded the rocks and coincided with a marked change in the tectonic environment. Shocks from earthquakes and volcanic explosions in the new tectonic environment caused brecciation in mafic and felsic sills and partial melting of felsic rocks. The low-temperature metamorphism and the tectonic disturbances ended with emplacement of the ophiolite into the continental margin.

Remaining Problems

Although this investigation has concluded with a detailed and probably reasonable sequence of events for the formation of an ophiolite, many of the formational events are presupposed without direct evidence for their occurrence. First, melting in mantle rocks must be presumed at various stages in development of the ophiolite suite but there is no indication why the melting occurred or what mechanism would have produced a series of basic melts that are all so similar in composition. This is the same question that arises at any place where large amounts of basaltic lavas are extruded, such as Hawaii, and along the mid-ocean ridges. Second, there was a marked change in environmental conditions, from high- to low-temperature. Although this was probably due to the inception or acceleration of crustal spreading, the cause of the spreading and changes in spreading

rates is not known. Third, the effects of intense tectonism in the San Luis Obispo rocks were highly localized within portions of the rock units. Why these effects should be so restricted is not understood, although occurrences of similar effects in lunar rocks, where intense deformation of impacting meteorites is common, are currently under investigation (Wilshire, pers. comm.), and may ultimately aid in interpreting the terrestrial case.

The problems in reconciling many details of ophiolite structure and chemistry to that of ocean crust and mantle remain, but this study indicates that the thinness and the Na-rich character of ophiolite bodies are not major obstacles to interpreting them as oceanic rocks. The history of ophiolites is obviously so complex, and the mode of emplacement so disruptive that the preservation of any original structures or layering is fortuitous. The process of Na-Si-metasomatism must occur characteristically in oceanic ridge areas, within the oceanic crust, but it does not entirely obscure the tholeiitic affinity of this ophiolite assemblage. However, the source of the Na and Si is unknown. The relationship between ultramafic and basic rocks of most ophiolites, including the San Luis Obispo body, is still a major difficulty. Although it is now certain that many ultramafic rocks of ophiolites are depleted mantle and that many others represent portions of stratiform cumulate complexes, the ultramafic parent material is still a hypothetical material.

APPENDIX I

Electron Probe Microanalyses of Minerals

Three hundred sixty-eight silicate mineral grains were analyzed for major element compositions using an ARL electron probe microanalyzer. The accelerating voltage for all analyses was 15 KV; sample currents varied from 3 to 5 x 10^{-8} amps, depending on the volatile content of the minerals being analyzed.

Mafic minerals olivine, pyroxene, amphibole and chlorite were analyzed for eight elements, which constitute 98 to 100 percent of the non-volatile composition. The eight elements are Si, Al, Fe, Ti, Mg, Ca, Na and K. K-alpha lines were used in the analyses of all elements.

Standards used were: (1) Kakanui augite, a homogeneous pyroxene for all the mafic minerals; (2) Crystal Bay bytownite for plagioclases; (3) epidote from Garnet Hill, Calaveras County, California, with slight Fe-Al inhomogeneity, for epidotes. Chlorites and epidotes were analyzed with a beam of 10 to 20 microns diameter to avoid excessive loss of volatiles and decrepitation of the sample.

Several 10 second counts were made on each spot, and numerous spots were probed in each grain to test for homogeneity. Precision of the duplicate counts was ±3 percent for most elements.

Data were reduced using the MAGIC program for matrix corrections written by J. W. Colby.

APPENDICES

The tables that follow contain data of pyroxene, amphibole, plagioclase, chlorite and epidote analyses. Amphibole and chlorite analyses are difficult to interpret for reliability. The totals range from 86 percent to over 101 percent, in minerals that are obviously highly altered. The highest totaled analyses were discarded in plotting data, but the low totals were used. Low totals in amphiboles were produced in analytical runs that also produced good pyroxene analyses. This result is taken to mean that the low totals are due to alteration and are a real composition of the phases probed.

Appendix Ia

Electron Probe Analyses of Pyroxenes

A. Ultramafic xenoliths

	(1) P7068X Feldspathic peridotite		(2) P7080 Lherzolite (C, table 1a)			
Wt. %	CP2	CP3	A1A	A1B	B1B	C2
SiO_2	56.5	56.0	54.4	54.2	53.9	53.7
TiO_2	0.2	0.1	0.7	0.6	0.8	0.8
Al_2O_3	1.6	1.3	3.2	3.1	3.2	3.0
FeO*	5.3	5.1	5.6	5.7	5.9	5.7
MgO	17.2	17.6	16.8	16.5	16.8	14.8
CaO	22.4	23.6	21.3	22.0	22.4	22.7
Na_2O	0.3	0.4	0.3	0.3	0.4	0.4
K_2O	0.2	0.2	0.0	0.0	0.0	0.0
Total	103.7	104.3	103.4	102.3	102.4	101.1
Calculated compositions	$En_{51}Fs_{0.8}Wo_{48}$		$En_{47}Fs_9Wo_{44}$		$En_{43}Fs_9Wo_{48}$	

B. In situ cumulate ultramafic rocks

C. Multistage gabbro (13, table 11b)

	(3) wehrlite (E, table 1a)		
Wt. %	M22	CE2	CE2P
SiO_2	55.9	54.7	52.0
TiO_2	0.3	0.4	0.4
Al_2O_3	2.2	2.5	2.9
FeO*	4.3	6.9	7.3
MgO	16.7	14.8	15.8
CaO	19.0	22.4	21.7
Na_2O	0.2	0.2	0.2
K_2O	0.2	0.0	0.0
Total	98.8	101.9	100.3
Calculated compositions	$En_{50}Fs_{\cancel{57}\,8}Wo_{42}$	$En_{44}Fs_{12}Wo_{44}$	

Appendix Ia (cont'd.)

D. Diabasic sill, Cuesta Ridge intrusive complex

Wt. %	OB1	OC1
SiO_2	54.0	54.2
TiO_2	0.3	0.2
Al_2O_3	3.6	3.8
FeO*	12.6	12.5
MgO	15.7	16.3
CaO	11.5	11.7
Na_2O	0.3	0.3
K_2O	1.8	1.6
Total	99.7	100.6
Calculated composition	$En_{50}Fs_{23}Wo_{27}$	

Appendix Ib

Electron Probe Analyses of Amphiboles

A. Amphiboles in ultramafic xenoliths

(1) Feldspathic xenoliths

	P7068X		P70216		
Wt. %	CAM1	CAM2	1B1	2A	2B
SiO_2	49.6	48.8	44.8	46.1	43.5
TiO_2	1.5	1.6	3.1	2.5	2.3
Al_2O_3	7.1	7.6	9.8	9.9	9.8
FeO*	8.3	8.5	0.9	1.0	0.9
MgO	8.5	8.4	15.3	15.4	15.4
CaO	11.6	11.6	11.4	11.8	11.9
Na_2O	1.7	1.8	2.6	1.8	2.0
K_2O	2.4	2.3	1.8	2.3	1.8
Total	90.7	90.6	89.7	90.8	87.6

Structural Formulae[1]

Si	7.6		7.6		6.8		6.9		6.8	
Al(IV)	0.4	8.0	0.4	8.0	1.2	8.0	1.1	8.0	1.2	8.0
Al(VI)	0.9		0.9		0.6		0.6		0.6	
Ti	0.2		0.2		0.4		0.6		0.3	
Fe^{+2}	1.1	4.2	1.1	4.1	0.1	4.5	0.1	4.7	0.1	4.6
Mg	2.0		1.9		3.4		3.4		3.6	
Ca	1.9		1.9		1.8		1.9		2.0	
Na	0.4	2.7	0.5	2.6	0.8	3.0	0.5	2.8	0.6	2.8
K	0.4		0.2		0.4		0.4		0.2	

[1]Calculated relative to 23 oxygen atoms

Appendix Ib (cont'd.)

(2) Lherzolite xenolith (C, table 1a)

P7080

Wt. %	A1C	B1A
SiO_2	44.2	44.2
TiO_2	3.7	3.6
Al_2O_3	11.2	11.1
FeO*	7.2	7.3
MgO	7.8	8.3
CaO	12.6	12.3
Na_2O	1.8	2.6
K_2O	0.0	0.0
Total	88.5	89.4

Structural Formulae

Si	6.9	8.0	6.9	8.0
Al(IV)	1.1		1.1	
Al(VI)	0.9		0.9	
Ti	0.4	4.0	0.4	4.2
Fe^{+2}	0.9		1.0	
Mg	1.8		1.9	
Ca	2.1		2.0	
Na	0.5	2.6	0.8	2.8
K	0.0		0.0	

Appendix Ib (cont'd.)

B. Amphibolite and uralite gabbro, Cerro Alto intrusive complex

(1) Amphibolite (1, table 10)

Wt. %	CD11	CD21	CD22	CD23
SiO_2	47.1	47.7	47.1	47.6
TiO_2	1.4	1.3	1.4	1.5
Al_2O_3	7.5	7.2	7.6	7.5
FeO*	8.5	8.8	9.4	9.4
MgO	17.7	18.8	17.5	18.0
CaO	11.6	11.7	11.4	11.5
Na_2O	1.1	1.2	1.2	1.1
K_2O	0.8	0.4	0.8	0.7
Total	95.7	97.1	96.4	97.3

Structural Formulae

Si	6.9		6.9		6.9		6.9	
Al(IV)	1.1	8.0	1.1	8.0	1.1	8.0	1.1	8.0
Al(VI)	0.1		0.2		0.2		0.2	
Ti	0.1		0.1		0.2		0.2	
Fe^{+2}	1.1	5.2	1.1	5.4	1.2	5.4	1.1	5.4
Mg	3.9		4.0		3.8		3.9	
Ca	1.9		1.8		1.8		1.8	
Na	0.4	2.5	0.3	2.4	0.3	2.2	0.3	2.2
K	0.2		0.1		0.1		0.1	

Appendix Ib (cont'd.)

(1) Amphibolite (cont'd.)

Wt. %	CD24	CE22	CE31	CF21
SiO_2	48.0	47.4	48.6	46.6
TiO_2	1.4	1.4	1.4	1.7
Al_2O_3	7.5	7.4	7.5	8.0
FeO*	9.1	9.1	9.8	9.5
MgO	18.3	17.3	16.4	17.7
CaO	11.7	13.4	11.6	11.6
Na_2O	1.1	1.1	1.2	1.3
K_2O	0.7	0.7	0.7	0.7
Total	97.8	97.8	97.2	97.1

Structural Formulae

Si	6.9		6.8		7.0		6.8	
Al(IV)	1.1	8.0	1.2	8.0	1.0	8.0	1.2	8.0
Al(VI)	0.2		0.0		0.3		0.2	
Ti	0.2		0.2		0.2		0.2	
Fe^{+2}	1.1	5.4	1.1	5.0	1.2	5.2	1.2	5.4
Mg	3.9		3.7		3.5		3.8	
Ca	1.8		2.0		1.8		1.8	
Na	0.3	2.2	0.3	2.4	0.3	2.2	0.4	2.3
K	0.1		0.1		0.1		0.1	

Appendix Ib (cont'd.)

(2) Uralite gabbro, Cerro Alto intrusive complex (3, table 10)

Wt. %	CA2	CB11	CC1	CC2	CE11
SiO_2	50.3	50.4	49.3	49.4	46.2
TiO_2	1.6	1.8	2.0	1.7	2.2
Al_2O_3	7.6	8.0	8.3	7.6	8.5
FeO*	10.6	10.8	11.0	11.1	10.4
MgO	16.7	16.8	16.8	17.4	16.6
CaO	12.0	12.0	11.7	12.2	11.6
Na_2O	1.3	1.4	1.3	1.8	1.8
K_2O	0.9	0.8	0.8	0.8	0.7
Total	101.0	102.0	101.3	101.3	98.0

Structural Formulae

Si	7.0		7.0		6.9		6.9		6.7	
Al(IV)	1.0	8.0	1.0	8.0	1.1	8.0	1.1	8.0	1.3	8.0
Al(VI)	0.2		0.3		0.2		0.1		0.1	
Ti	0.2		0.2		0.4		0.2		0.2	
Fe^{+2}	1.2	5.1	1.2	5.2	1.3	5.4	1.3	5.2	1.3	5.2
Mg	3.5		3.5		3.5		3.6		3.6	
Ca	1.8		1.8		1.8		1.8		1.8	
Na	0.3	2.3	0.4	2.3	0.2	2.1	0.5	2.5	0.5	2.5
K	0.2		0.1		0.1		0.5		0.2	

Appendix Ib (cont'd.)

(2) Uralite gabbro (cont'd.)

Wt. %	CA11	CA21	CA22	CA23	CA31
SiO_2	51.6	52.9	53.9	52.9	50.4
TiO_2	0.6	0.9	0.6	0.8	1.4
Al_2O_3	4.1	5.2	8.2	4.5	6.2
FeO*	9.8	10.0	6.2	8.9	7.8
MgO	8.2	8.4	8.5	9.0	8.7
CaO	12.3	11.8	12.4	12.1	12.7
Na_2O	0.8	0.8	1.8	0.6	0.6
K_2O	2.1	1.7	1.4	1.6	1.4
Total	89.5	91.7	93.0	90.4	89.2

Structural Formulae

Si	8.4		8.0		7.9		8.1		7.8	
Al(IV)	0.0	8.4	0.0	8.0	0.1	8.0	0.0	8.1	0.2	8.0
Al(VI)	0.8		1.0		1.3		0.8		0.9	
Ti	0.2		0.1		0.1		0.1		0.2	
Fe^{+2}	1.3	4.3	1.3	4.3	0.8	4.0	1.1	4.0	1.0	4.1
Mg	2.0		1.9		1.8		2.0		2.0	
Ca	2.1		1.9		1.9		2.0		2.1	
Na	0.2	2.7	0.2	2.5	0.4	2.5	0.2	2.6	0.2	2.5
K	0.4		0.4		0.2		0.4		0.2	

Appendix Ib (cont'd.)

(2) Uralite gabbro (cont'd.)

Wt. %	CA32	CA41	CA42	CA43
SiO_2	53.0	53.3	53.2	50.8
TiO_2	0.5	0.7	0.7	0.5
Al_2O_3	3.8	4.2	5.5	5.3
FeO*	9.3	10.1	8.0	7.4
MgO	8.6	8.5	8.3	8.8
CaO	12.2	11.8	13.8	12.2
Na_2O	0.7	0.7	0.6	0.7
K_2O	1.6	1.8	1.4	1.1
Total	89.8	91.1	91.5	86.8

Structural Formulae

Si	8.2		8.1		8.0		8.0	
Al(IV)	0.0	8.2	0.0	8.1	0.0	8.0	0.0	8.0
Al(VI)	0.6		0.8		1.0		1.0	
Ti	0.0		0.1		0.1		0.0	
Fe^{+2}	1.2	3.8	1.3	4.1	1.0	4.0	1.0	4.1
Mg	2.0		1.9		1.9		2.1	
Ca	1.0		1.9		2.2		2.1	
Na	0.2	2.4	0.2	2.5	0.2	2.6	0.2	2.5
K	0.2		0.4		0.2		0.2	

Appendix Ib (cont'd.)

C. Amphiboles from multistage gabbros, Cuesta Ridge intrusive complex

	(1) Gabbro (15, table 11b)		(2) Gabbro (16, table 11b)			
Wt. %	CE1		1BA		1CA	
SiO_2	55.3		49.0		51.1	
TiO_2	0.4		1.4		0.3	
Al_2O_3	2.2		4.8		5.0	
FeO*	10.9		1.1		1.0	
MgO	8.4		16.1		17.0	
CaO	12.1		11.9		11.8	
Na_2O	0.3		0.9		0.5	
K_2O	0.0		1.4		0.4	
Total	89.6		86.6		87.1	

Structural Formulae

Si	8.5		7.6		7.8	
Al(IV)	0.0	8.5	0.4	8.0	0.2	8.0
Al(VI)	0.4		0.5		0.7	
Ti	0.0		0.2		0.0	
Fe^{+2}	1.4	3.7	0.1	4.5	0.1	4.6
Mg	1.9		3.7		3.8	
Ca	2.0		2.0		1.9	
Na	0.1	2.1	0.2	2.4	0.2	2.2
K	0.0		0.2		0.2	

Appendix Ib (cont'd.)

(2) Gabbro (cont'd.)

Wt. %	2AA	2AB	2BA	2BB
SiO_2	49.9	50.3	50.2	49.5
TiO_2	1.1	1.1	1.3	1.3
Al_2O_3	4.6	5.2	4.5	5.2
FeO*	1.1	1.1	1.1	1.1
MgO	16.3	16.0	16.5	16.0
CaO	11.8	11.7	11.6	11.9
Na_2O	0.8	0.7	0.7	0.8
K_2O	1.4	1.4	1.4	1.4
Total	87.0	87.5	87.3	87.2

Structural Formulae

Si	7.7		7.7		7.7		7.6	
Al(IV)	0.3	8.0	0.3	8.0	0.3	8.0	0.4	8.0
Al(VI)	0.5		0.7		0.5		0.5	
Ti	0.1		0.1		0.1		0.2	
Fe^{+2}	0.1	4.4	0.1	4.5	0.1	4.5	0.1	4.5
Mg	3.7		3.6		3.8		3.7	
Ca	1.9		1.9		1.9		2.0	
Na	0.2	2.3	0.2	2.3	0.2	2.3	0.2	2.4
K	0.2		0.2		0.2		0.2	

Appendix Ib (cont'd.)

D. Cumulate gabbros, Cuesta Ridge intrusive complex

(1) (13, table 11b)

Wt. %	C1A1	C1A2	C1A3	C1C2	C2B3
SiO_2	51.4	49.5	48.8	52.5	49.9
TiO_2	0.8	1.5	2.0	0.4	1.6
Al_2O_3	4.6	6.4	6.3	3.8	5.2
FeO*	10.8	10.4	9.8	10.8	12.9
MgO	16.6	16.7	17.1	17.8	15.4
CaO	11.4	11.6	11.8	11.5	11.1
Na_2O	1.3	1.3	1.5	0.6	1.2
K_2O	1.8	1.7	1.7	1.2	2.0
Total	98.7	99.1	99.0	98.6	99.3

Structural Formulae

Si	7.4		7.1		6.7		7.5		7.2	
Al(IV)	0.6	8.0	0.9	8.0	1.0	7.7	0.5	8.0	0.8	8.0
Al(VI)	0.2		0.2		0.0		0.1		0.1	
Ti	0.1		0.2		0.2		0.0		0.2	
Fe^{+2}	1.3	5.1	1.2	5.2	1.1	4.7	1.3	5.2	1.6	5.2
Mg	3.5		3.6		3.5		3.8		3.3	
Ca	1.7		1.8		1.7		1.8		1.7	
Na	0.4	2.4	0.4	2.5	0.4	2.4	0.2	2.2	0.3	2.4
K	0.3		0.3		0.3		0.2		0.4	

Appendix Ib (cont'd.)

	(1) (cont'd.)	(2) (14, table 11b)		
			same grain	
Wt. %	C1B2	H1A	H1B1	H1B2
SiO_2	42.4	51.5	51.5	54.4
TiO_2	0.3	1.2	0.8	0.3
Al_2O_3	7.0	5.3	4.4	2.4
FeO*	9.1	7.8	8.1	9.8
MgO	15.4	17.8	17.2	19.5
CaO	9.3	11.0	11.0	8.3
Na_2O	0.4	1.5	0.7	0.3
K_2O	2.4	1.5	1.4	1.0
Total	86.3	97.6	95.2	96.0

Structural Formulae

Si	7.0		7.3		7.5		7.8	
Al(IV)	1.0	8.0	0.7	8.0	0.5	8.0	0.2	8.0
Al(VI)	0.4		0.2		0.3		0.2	
Ti	0.0		0.1		0.1		0.0	
Fe^{+2}	1.2	5.4	0.9	5.0	1.0	5.1	1.2	5.6
Mg	3.8		3.8		3.7		4.2	
Ca	1.6		1.6		1.7		1.3	
Na	0.1		0.4		0.2		0.1	
K	0.5		0.3		0.3		0.2	

Appendix Ib (cont'd.)

(2) (cont'd.)

	same grain			same grain	
Wt. %	H1C1	H1C2	H1C3	H1D1	H1D2
SiO_2	52.8	52.0	52.3	49.8	49.8
TiO_2	0.6	0.9	0.9	0.2	0.2
Al_2O_3	4.1	4.4	4.5	2.0	3.0
FeO*	7.6	7.7	8.1	9.0	6.5
MgO	18.6	18.4	17.8	18.2	18.0
CaO	11.1	11.1	11.3	2.3	8.7
Na_2O	1.0	1.1	1.2	0.1	0.6
K_2O	1.1	1.4	1.3	0.3	1.0
Total	96.9	97.0	97.4	81.9	87.8

Structural Formulae

Si	7.5		7.4		7.4		8.1		7.7	
Al(IV)	0.5	8.0	0.6	8.0	0.6	8.0	0.0	8.1	0.3	8.0
Al(VI)	0.2		0.1		0.2		0.4		0.1	
Ti	0.1		0.1		0.1		0.0		0.0	
Fe^{+2}	0.9	5.1	0.9	5.1	1.0	5.2	1.2	6.0	0.8	5.1
Mg	3.9		3.9		3.8		4.4		4.2	
Ca	1.7		1.7		1.7		0.4		1.4	
Na	0.3		0.3		0.3		0.0	0.6	0.2	1.8
K	0.2		0.2		0.2		0.1		0.2	

Appendix Ib (cont'd.)

(2) (cont'd.)

Wt. %	H21	J1A1	JLA2	J1A3
SiO_2	54.2	51.9	54.1	51.6
TiO_2	0.3	1.5	1.0	1.7
Al_2O_3	2.5	5.9	4.2	6.1
FeO*	7.9	9.6	9.1	9.5
MgO	18.2	17.0	18.6	17.2
CaO	11.0	12.1	12.3	11.6
Na_2O	0.5	1.4	1.0	1.5
K_2O	1.3	1.9	1.9	2.3
Total	95.9	101.3	102.2	101.5

Structural Formulae

Si	7.8		7.2		7.4		7.2	
Al(IV)	0.2	8.0	0.8	8.0	0.6	8.0	0.8	8.0
Al(VI)	0.2		0.2		0.1		0.2	
Ti	0.0		0.2		0.1		0.2	
Fe^{+2}	0.9	5.0	1.1	5.0	1.0	5.0	1.1	5.1
Mg	3.9		3.5		3.8		3.6	
Ca	1.7		1.8		1.8		1.7	
Na	0.1	2.0	0.4	2.5	0.3	2.4	0.4	2.5
K	0.2		0.3		0.3		0.4	

Appendix Ib (cont'd.)

(2) (cont'd.)

Wt. %	J1B1	J1B2
SiO_2	52.7	54.5
TiO_2	1.3	0.6
Al_2O_3	5.6	4.0
FeO*	9.6	9.0
MgO	17.6	18.6
CaO	12.7	12.0
Na_2O	1.5	0.8
K_2O	1.4	1.4
Total	102.4	100.9

Structural Formulae

Si	7.2		7.6	
Al(IV)	0.8	8.0	0.4	8.0
Al(VI)	0.1		0.2	
Ti	0.1		0.1	
Fe^{+2}	1.1	4.9	1.0	5.0
Mg	3.6		3.7	
Ca	1.9		1.8	
Na	0.4	2.5	0.2	2.2
K	0.2		0.2	

Appendix Ib (cont'd.)

E. Amphiboles in diabase and diorite of the Cuesta Ridge intrusive complex

(1) Diabase (9, table 11a)

Wt. %	A1	A2	A3	B1
SiO_2	49.8	50.5	49.0	50.8
TiO_2	0.0	0.1	0.3	0.4
Al_2O_3	5.1	5.7	6.7	5.9
FeO*	14.8	14.1	8.9	14.8
MgO	3.0	15.3	12.3	14.9
CaO	11.3	10.9	6.7	8.4
Na_2O	0.4	0.4	4.4	0.4
K_2O	3.0	3.3	1.7	5.6
Total	87.4	100.3	90.0	101.2

Structural Formulae

Si	8.2		7.2		7.6		7.3	
Al(IV)	0.0	8.2	0.8	8.0	0.4	8.0	0.7	8.0
Al(VI)	1.0		0.2		0.8		0.3	
Ti	0.0		0.0		0.0		0.0	
Fe^{+2}	2.0	3.7	1.7	5.2	1.2	4.8	1.8	5.3
Mg	0.7		3.3		2.8		3.2	
Ca	2.0		1.7		1.1		1.3	
Na	0.1	2.7	0.1	2.4	0.3	2.7	0.1	2.4
K	0.6		0.6		0.3		1.0	

Appendix Ib (cont'd.)

(1) Diabase (cont'd.)

Wt. %	B2	B3	C1	C2
SiO_2	53.9	50.0	48.9	51.9
TiO_2	0.5	0.2	0.2	0.1
Al_2O_3	4.2	5.7	7.0	4.7
FeO*	14.0	15.2	16.2	14.2
MgO	13.3	15.4	16.7	14.8
CaO	13.0	5.9	11.0	12.6
Na_2O	0.4	0.2	0.3	0.4
K_2O	1.2	5.5	2.5	2.7
Total	100.5	98.1	102.8	101.4

Structural Formulae

Si	7.6		7.4		6.9		7.4	
Al(IV)	0.4	8.0	0.6	8.0	1.1	8.0	0.6	8.0
Al(VI)	0.3		0.4		0.1		0.1	
Ti	0.0		0.0		0.0		0.0	
Fe^{+2}	1.7	4.8	1.9	5.7	1.9	5.5	1.7	4.9
Mg	2.8		3.4		3.5		3.1	
Ca	2.0		0.9		1.7		1.9	
Na	0.1	2.3	0.0	1.9	0.1	2.2	0.1	2.5
K	0.2		1.0		0.4		0.5	

Appendix Ib (cont'd.)

(2) Diorite from Cuesta Ridge intrusive complex

Wt. %	GB1-2	GB2	GB3-1	GB3-2
SiO_2	46.3	47.9	47.2	44.1
TiO_2	0.1	0.1	0.1	0.2
Al_2O_3	11.7	8.0	8.9	6.1
FeO*	12.0	10.3	10.5	10.1
MgO	16.8	13.9	15.0	14.2
CaO	13.4	7.0	7.1	6.9
Na_2O	0.3	0.4	0.6	0.3
K_2O	0.8	1.0	0.8	0.9
Total	101.4	88.6	90.2	84.8

Structural Formulae

Si	6.2		7.8		7.6		7.7	
Al(IV)	1.8	8.0	0.2	8.0	0.4	8.0	0.3	8.0
Al(VI)	0.0		1.3		1.3		0.9	
Ti	0.0		0.0		0.0		0.0	
Fe^{+2}	1.3	4.7	1.4	6.1	1.4	6.3	1.5	6.1
Mg	3.4		3.4		3.6		3.7	
Ca	1.9		1.2		1.2		1.3	
Na	0.1	2.1	0.1	1.5	0.2	1.6	0.1	1.6
K	0.1		0.2		0.2		0.2	

Appendix Ic

Electron Probe Analyses of Plagioclases

Sample	SiO_2	Al_2O_3	FeO*	CaO	Na_2O	K_2O	Total	An content
1. 7271, amphibolite (1, table 10)								
CB21	47.9	33.0	0.0	17.6	1.8	0.1	100.4	87
CB123	47.9	33.0	0.0	17.8	2.2	0.1	101.0	88
CF32	44.7	33.2	0.0	17.4	0.1	0.1	95.5	86
CE13	45.5	28.1	0.0	16.8	1.8	0.1	92.3	84
2. 7219G, diabase sill (8, table 11a)								
1-3	67.9	21.1	0.4	2.2	10.7	0.1	102.4	11
2-1	67.9	20.9	0.4	1.8	10.8	0.1	101.9	9
3. P7031V, diabase dike (G, table 1b)								
3111	49.4	31.9	0.5	16.5	2.3	0.2	100.8	82
4. P70216, feldspathic cumulate xenolith (D, table 1a)								
1-A	52.9	29.2	0.4	11.4	4.9	0.5	99.3	57
1B-2	52.4	29.7	0.4	20.8	5.6	0.5	99.4	54
1C31	54.9	27.8	0.3	9.9	5.7	0.6	99.2	49
1C32	54.9	28.7	0.3	9.9	5.2	0.3	99.3	49

Appendix Ic (cont'd.)

Sample	SiO_2	Al_2O_3	FeO*	CaO	Na_2O	K_2O	Total	An content
5. 7222C, quartz-albitite								
C2A1	66.4	22.0	0.1	0.8	10.9	0.4	100.6	4
C2A2	65.8	22.0	0.1	1.0	10.4	0.6	99.9	5
C2B1	60.3	25.6	0.3	5.6	7.8	0.7	100.3	28
C2B2	63.5	22.5	0.2	0.2	11.8	0.1	98.3	1
C2C2	66.2	21.6	0.1	2.0	10.5	0.1	100.5	10
C2C1	64.7	22.1	0.1	1.0	9.3	1.3	98.5	5
C2B2	67.2	21.5	0.1	0.2	11.7	0.1	100.8	1
6. 7222H, cumulate gabbro (13, table 11b)								
H1E	64.9	21.1	0.2	1.4	10.0	0.2	97.8	7
7. 7222J, cumulate gabbro (14, table 11b)								
J1A4	62.0	24.5	0.6	5.8	7.4	0.6	100.9	29
J1A5-1	68.1	20.8	0.2	1.3	10.4	0.2	101.0	6
J1A5-2	63.9	23.7	0.3	4.4	8.1	0.6	101.0	22
J2C1	58.6	26.9	0.6	9.1	6.2	0.4	101.8	45

Appendix Ic (cont'd.)

Sample	SiO_2	Al_2O_3	FeO*	CaO	Na_2O	K_2O	Total	An content
8. 7222Ø, metamorphosed diabase								
ØA3	60.5	23.0	1.2	6.9	4.5	0.2	96.3	34
ØC2	76.5	14.0	0.3	1.7	3.4	3.8	99.7	8
ØC41	81.6	9.5	0.8	2.4	2.0	2.0	98.3	12
Ø85-1	62.4	23.1	0.7	2.0	8.9	1.3	98.4	10
Ø85-2	68.7	19.2	0.8	1.2	9.1	0.4	99.4	6
9. 7222S, diabasic sill (9, table 11a)								
A-5	67.7	21.0	0.2	1.4	10.9	0.1	101.3	7
A-6	67.6	21.4	0.2	1.0	10.5	0.6	101.3	5
C-4	68.1	20.6	0.2	1.3	10.7	0.2	101.1	6
10. 7224A, quartz-diorite								
AA1	58.5	25.3	0.5	7.2	7.5	0.1	99.1	36
AB2	56.1	26.8	0.4	8.8	6.4	0.1	98.6	44
AC1	59.5	25.3	0.3	7.4	7.5	0.1	100.1	37
AC2	57.3	26.2	0.3	8.0	6.5	0.1	98.4	40

Appendix Ic (cont'd.)

Sample	SiO_2	Al_2O_3	FeO*	CaO	Na_2O	K_2O	Total	An content
11. 7229G, altered quartz-diorite								
GB1	53.5	26.6	0.4	6.6	7.4	0.1	94.6	33
GB2C	53.3	27.0	0.4	8.2	6.5	0.2	95.6	40
GA2	54.5	27.0	0.4	5.4	8.4	0.1	95.8	27
GA3	55.5	26.3	0.4	7.0	7.1	0.2	96.5	35
GC-1	54.0	27.7	0.4	8.6	6.6	0.1	97.4	43
GC1-2	54.0	27.6	0.4	5.8	7.2	0.7	95.7	29
12. 7232A, quartz-albitite								
32A1	69.3	20.0	0.1	0.3	11.7	0.2	101.6	1
32A2-1	68.8	19.8	0.1	1.1	11.3	0.2	101.4	5
32A2-2	61.5	20.9	1.7	1.1	11.6	0.2	97.0	5
32A3	69.3	20.1	0.1	0.4	11.5	0.3	101.3	2
32B	68.7	19.8	0.3	1.5	10.4	0.2	100.9	7
32C1	68.7	19.9	0.2	0.4	11.2	0.1	100.5	2
32C2	68.1	20.1	0.2	1.2	10.9	0.5	101.0	6
32D1	68.8	20.1	0.1	0.3	11.8	0.1	101.2	5
32D2-1	66.1	21.4	0.3	0.3	11.3	0.4	99.8	5
32D2-2	68.7	19.8	0.1	0.3	11.2	0.4	100.5	5

Appendix Ic (cont'd.)

Sample	SiO_2	Al_2O_3	FeO*	CaO	Na_2O	K_2O	Total	An content
13. 7234B, quartz-albitite, all with low Ca values								
A22-1	63.0	18.9	0.5	0.2	11.2	0.1	93.9	1
A22-2	63.5	18.9	0.2	0.6	11.0	0.1	94.3	3
B31-1	66.0	17.1	0.1	0.4	11.0	0.1	94.7	2
B31-2	72.3	11.6	0.2	0.2	5.9	0.1	90.3	1 (highly altered)
B32	64.6	19.0	0.1	0.2	11.2	0.1	95.2	1
C31-1	66.9	17.2	0.2	1.9	10.0	0.1	96.3	9
C31-2	67.3	17.2	0.1	0.2	11.7	0.1	96.6	1
C33	61.3	19.1	1.3	0.3	11.1	0.1	93.2	1
C32	60.7	19.3	1.3	0.3	11.2	0.2	93.0	1
14. 7234C, quartz-albitite								
34C1	70.2	18.6	0.2	0.3	11.3	0.3	100.9	1
34C5-1	66.1	21.4	0.2	1.3	10.8	0.3	100.1	6
34C5-2	65.3	20.0	1.0	0.6	9.3	1.4	97.6	3
15. 7236F2, quartz-albitite								
F2A2	68.5	21.7	0.1	0.7	9.5	0.2	100.7	3
F2B1	66.8	22.2	0.3	0.6	10.1	0.3	100.3	3

Appendix Ic (cont'd.)

Sample	SiO_2	Al_2O_3	FeO*	CaO	Na_2O	K_2O	Total	An content
16. 7237B, quartz-albitite								
BA1	65.6	20.7	0.3	0.8	10.8	0.4	98.6	4
BA2-1	63.9	20.8	0.6	1.3	9.9	0.7	97.2	6
BA2-2	65.0	20.8	0.7	0.7	10.4	0.6	98.2	3
BA2-3	65.6	20.6	0.4	0.3	11.3	0.4	98.6	1
BA3	65.4	20.5	0.4	0.5	10.6	0.5	97.9	2
BB1-1	65.9	20.7	0.2	0.5	10.8	0.5	98.6	2
BB1-2	65.9	20.7	0.2	0.7	10.8	0.5	98.8	3
BB1-3	65.8	20.5	0.2	1.4	10.3	0.6	98.8	7
BB1-4	66.1	19.9	0.0	7.4	7.6	0.5	101.5	37
BB1-5	66.9	19.8	0.1	0.2	10.1	0.1	97.2	1
BC1	64.9	21.9	0.2	0.9	10.6	0.5	99.0	4
BC2	71.2	17.9	0.1	0.4	11.0	0.2	100.8	2
17. 7240E, quartz-albitite								
EC1	67.0	20.0	0.8	0.4	11.6	0.3	100.1	2

Appendix Ic (cont'd.)

Sample	SiO_2	Al_2O_3	FeO*	CaO	Na_2O	K_2O	Total	An content
18. 7240F, granophyric quartz-albitite								
FA1-1	67.6	20.8	0.1	0.2	12.9	0.1	101.7	1
FA1-2	67.4	20.8	0.1	0.6	12.1	0.4	101.4	3
FA2	64.8	21.1	0.5	1.0	12.1	0.3	99.8	5
FB1	67.2	21.1	0.2	0.4	12.9	0.1	101.9	2
FB2-1	65.3	21.5	0.3	0.8	12.7	0.3	100.9	4
FB2-2	67.2	21.4	0.1	0.6	12.0	0.6	101.9	3
FD1	67.8	20.8	0.1	0.6	11.0	0.2	100.6	3
FD2	67.8	20.5	0.1	0.6	10.4	0.1	99.5	3
FD4-1	68.3	21.6	0.1	0.6	10.4	0.1	101.1	3
FD4-2	68.8	21.3	0.2	0.5	9.4	0.6	100.8	2
19. 7241D, altered quartz-albitite								
DA1-1	67.7	20.8	0.2	0.5	9.9	0.3	99.4	2
DA1-2	67.4	20.6	0.2	0.4	8.1	1.1	97.8	2
DA2	68.6	19.9	0.0	0.4	10.1	0.1	99.1	2
DA3	67.0	20.9	0.2	0.4	9.9	0.2	98.6	2
DB1-1	66.2	21.1	0.5	1.1	9.9	0.2	99.0	5
DB1-2	66.3	21.2	0.5	0.6	10.3	0.1	99.0	3

Appendix Ic (cont'd)

Sample	SiO_2	Al_2O_3	FeO*	CaO	Na_2O	K_2O	Total	An content
20. 7241E, garnet-bearing "diorite" (21, table 14)								
2A1-1	65.6	19.3	0.0	0.2	11.6	0.2	96.9	1
2A1-2	64.3	19.9	0.1	0.2	10.4	0.6	95.5	1
2A1-3	63.1	21.6	0.2	0.3	11.1	0.3	96.6	1
2B1-1	65.6	19.3	0.0	0.3	11.9	0.1	97.2	1
2B1-2	65.6	19.7	0.1	0.3	11.6	0.2	97.5	1
2B1-3	63.9	20.3	0.1	0.2	10.4	0.5	95.4	1
2B2	63.9	20.1	0.1	0.3	11.2	0.3	95.9	1
2C2	64.0	20.6	0.1	0.2	11.3	0.3	96.5	1
2C3	64.7	20.2	0.0	0.2	11.2	0.3	96.6	1
21. 7244C, garnet-bearing "diorite" (another sample)								
C1BA	67.4	20.9	0.2	1.1	10.7	0.4	100.7	5
C1BB	64.0	20.3	1.3	0.5	11.4	0.4	97.9	2
C1BC	67.1	20.9	0.2	0.8	10.4	0.2	99.6	4
C2BA	67.0	20.6	0.2	0.6	11.0	0.2	99.6	3
C2BB-1	67.4	20.1	0.2	0.6	10.9	0.3	99.5	3
C2BC	66.5	20.2	0.4	0.6	11.2	0.2	99.1	3
C2CA	68.1	20.3	0.3	0.6	11.7	0.1	101.1	3

Appendix Ic (cont'd.)

Sample	SiO_2	Al_2O_3	FeO*	CaO	Na_2O	K_2O	Total	An content
22. 7245C, quartz-albitite								
CA1	67.8	20.2	0.0	0.5	10.0	0.2	98.7	2
CA2	67.8	20.1	0.1	0.3	10.2	0.2	98.7	1
CC1	66.6	19.9	0.0	0.3	10.5	0.1	97.4	1
CC2	66.0	20.8	0.2	0.3	10.3	0.2	97.8	1
CC3	68.1	20.4	0.1	0.3	10.4	0.2	99.5	1
23. 7257l, quartz-albitite								
57A1	69.5	20.6	0.1	0.2	10.7	0.1	101.2	1
57A2	68.0	20.6	0.1	0.4	10.1	0.2	99.4	2
57B2	68.3	20.9	0.1	0.7	10.0	0.4	100.4	3
24. 7277P1, altered quartz-diorite								
PC1	63.0	21.9	0.1	1.7	9.6	0.7	97.0	8
PC21	64.9	20.6	0.1	1.0	9.9	0.8	97.3	8
PC22	63.8	21.0	0.2	2.2	10.1	0.5	97.8	11
PC3-1	63.9	20.6	0.4	1.6	9.7	0.6	96.8	8
PC3-2	62.8	21.4	0.1	5.8	8.9	0.8	99.8	29
PC4-1	66.3	20.1	0.1	0.8	10.5	0.5	98.3	4

Appendix Id

Electron Probe Analyses of Chlorites

A. Diabasic intrusion from Cuesta Ridge intrusive complex

(1) Diabase with metamorphic texture

Wt. %	OA1	OA2	OA3	OD1	OD2C
SiO_2	28.2	28.2	28.3	30.6	32.4
TiO_2	0.1	0.1	0.1	0.1	0.1
Al_2O_3	20.7	19.9	20.5	19.4	18.0
FeO*	19.3	19.3	19.3	19.2	18.6
MgO	20.1	20.1	20.1	20.3	19.5
CaO	0.6	0.5	0.8	1.0	2.3
Na_2O	0.2	0.1	0.1	0.1	0.1
K_2O	0.9	1.1	0.7	1.6	1.6
Total	90.1	89.3	89.9	92.3	92.6

Structural Formulae

Si	2.8		2.8		2.8		3.0		3.1	
Al(IV)	1.2	4.0	1.2	4.0	1.2	4.0	1.0	4.0	0.9	4.0
Al(VI)	0.6		1.1		1.2		1.2		1.1	
Ti	0.0		0.0		0.0		0.0		0.0	
Fe^{+2}	1.6	5.5	1.6	5.7	1.6	5.8	1.6	5.8	1.5	5.6
Mg	3.0		3.0		3.0		2.9		2.8	
Ca	0.1		0.0		0.1		0.1		0.2	
Na	0.0		0.0		0.0		0.0		0.0	
K	0.1	0.1	0.1	0.1	0.1	0.1	0.2	0.2	0.2	0.2

Appendix Id (cont'd.)

(2) Sub-ophitic diabasic sill

Wt. %	A11	A12	A13	B11
SiO_2	25.4	25.3	25.4	23.0
TiO_2	0.0	0.0	0.0	0.0
Al_2O_3	19.4	20.2	20.5	18.3
FeO*	26.2	26.0	26.4	21.1
MgO	11.2	11.0	11.3	8.4
CaO	0.1	0.0	0.0	0.0
Na_2O	0.2	0.2	0.2	0.1
K_2O	1.0	0.9	0.9	0.7
Total	83.3	83.6	84.7	71.6

Structural Formulae

Si	2.8		2.8		2.8		3.0	
Al(IV)	1.2	4.0	1.2	4.0	1.2	4.0	1.0	4.0
Al(VI)	1.4		1.5		1.5		1.8	
Ti	0.0		0.0		0.0		0.0	
Fe^{+2}	2.5	5.8	2.4	5.7	2.4	5.7	2.3	5.7
Mg	1.9		1.8		1.8		1.6	
Ca	0.0		0.0		0.0		0.0	
Na	0.0		0.0		0.0		0.0	
K	0.1	0.1	0.1	0.1	0.1	0.1	0.1	0.1

Appendix Id (cont'd.)

(2) Sub-ophitic diabasic sill (cont'd.)

Wt. %	B12	B21	B22	C11
SiO_2	23.5	21.1	24.5	29.8
TiO_2	0.0	0.0	0.0	0.1
Al_2O_3	18.2	18.8	18.8	19.7
FeO*	22.2	22.1	23.2	22.4
MgO	9.8	11.6	12.6	12.9
CaO	0.1	0.2	0.0	0.1
Na_2O	0.1	0.2	0.3	0.3
K_2O	0.8	1.0	0.7	0.9
Total	74.7	75.0	80.1	86.2

Structural Formulae

Si	2.9		2.6		2.8		3.1	
Al(IV)	1.1	4.0	1.4	4.0	1.2	4.0	0.9	4.0
Al(VI)	1.5		1.3		1.4		1.5	
Ti	0.0		0.0		0.0		0.0	
Fe^{+2}	2.3	5.6	2.3	5.8	2.2	5.8	2.0	5.5
Mg	1.8		2.2		2.2		2.0	
Ca	0.0		0.0		0.0		0.0	
Na	0.0		0.0		0.1		0.1	
K	0.1	0.1	0.2	0.2	0.1	0.2	0.1	0.2

Appendix Id (cont'd.)

(2) Sub-ophitic diabasic sill (cont'd.)

Wt. %	C12	C2	D11	D12
SiO_2	25.0	24.9	25.3	25.4
TiO_2	0.1	0.0	0.0	0.0
Al_2O_3	19.7	19.6	19.6	20.5
FeO*	24.9	23.9	24.8	25.9
MgO	13.4	13.0	10.9	12.3
CaO	0.0	0.0	0.0	0.0
Na_2O	0.4	0.3	0.2	0.3
K_2O	0.7	0.9	0.9	0.8
Total	83.8	82.6	81.7	85.2

Structural Formulae

Si	2.8		2.8		2.9		2.8	
Al(IV)	1.2	4.0	1.2	4.0	1.1	4.0	1.2	4.0
Al(VI)	1.3		1.3		1.5		1.4	
Ti	0.0		0.0		0.0		0.0	
Fe^{+2}	2.3	5.8	2.2	5.7	2.4	4.7	2.4	5.8
Mg	2.2		2.2		1.8		2.0	
Ca	0.0		0.0		0.0		0.0	
Na	0.1		0.1		0.0		0.1	
K	0.0	0.1	0.1	0.2	0.2	0.2	0.1	0.2

Appendix Id (cont'd.)

B. Multistage "diorite" (21, table 14)

Wt. %	CGT1	CGT2	C2A2	C2A3
SiO_2	42.1	28.9	29.0	28.8
TiO_2	0.0	0.1	0.1	0.1
Al_2O_3	17.2	21.6	23.4	21.4
FeO*	11.5	19.2	17.7	20.1
MgO	10.6	16.5	16.3	17.7
CaO	0.3	1.4	0.1	0.1
Na_2O	1.5	0.2	0.3	0.2
K_2O	1.1	0.5	0.5	0.3
Total	84.3	88.4	87.4	88.7

Structural Formulae

Si	4.1		2.9		2.9		2.9	
Al(IV)	0.0	4.1	1.1	4.0	1.1	4.0	1.1	4.0
Al(VI)	2.0		1.5		1.7		1.4	
Ti	0.0		0.0		0.0		0.0	
Fe^{+2}	0.9	4.5	1.6	5.8	1.5	5.6	1.7	5.7
Mg	1.6		2.5		2.4		2.6	
Ca	0.0		0.2		0.0		0.0	
Na	0.3		0.1		0.1		0.0	
K	0.1	0.4	0.1	0.2	0.1	0.2	0.0	0.0

Appendix Id (cont'd.)

C. Diorites

(1)

Wt. %	3-1	3-2	3-3	3-4
SiO_2	24.2	25.5	25.1	25.1
TiO_2	0.1	0.1	0.1	0.1
Al_2O_3	4.7	21.6	21.0	21.4
FeO*	29.7	29.6	28.1	29.9
MgO	12.8	11.5	12.5	12.2
CaO	0.0	0.0	0.0	0.0
Na_2O	0.1	0.4	0.3	0.3
K_2O	0.9	1.6	1.9	1.3
Total	72.5	90.3	89.0	89.4

Structural Formulae

Si	3.3		2.7		2.7		2.7	
Al(IV)	0.5	4.0	1.3	4.0	1.3	4.0	1.3	4.0
Al(VI)	0.0		1.4		1.3		1.4	
Ti	0.0		0.0		0.0		0.0	
Fe^{+2}	3.4	6.0	2.6	5.8	2.5	5.8	2.6	5.9
Mg	2.6		1.8		2.0		1.9	
Ca	0.0		0.0		0.0		0.0	
Na	0.0		0.1		0.1		0.1	
K	0.2	0.2	0.2	0.3	0.2	0.3	0.2	0.3

Appendix Id (cont'd.)

(2) (cont'd.)

Wt. %	2-A	2-B	2-C
SiO_2	29.3	29.4	29.0
TiO_2	0.0	0.9	0.0
Al_2O_3	18.5	19.2	18.9
FeO*	14.2	14.4	14.6
MgO	23.1	23.1	21.9
CaO	0.0	0.0	0.1
Na_2O	0.2	0.2	0.2
K_2O	3.2	2.2	2.1
Total	88.5	89.4	86.8

Structural Formulae

Si	2.9		2.9		2.9	
Al(IV)	1.1	4.0	1.1	4.0	1.1	4.0
Al(VI)	1.1		1.1		1.1	
Ti	0.0		0.1		0.0	
Fe^{+2}	1.2	5.7	1.2	5.8	1.2	5.6
Mg	3.4		3.4		3.3	
Ca	0.0		0.0		0.0	
Na	0.0		0.0		0.0	
K	0.4	0.4	0.3	0.3	0.3	0.3

Appendix Ie

Electron Probe Analyses of Epidote from Quartz-Diorite and Quartz-Albitite[1]

	A				
Wt. %	OA21[2]	OA22	OA23	OA24	OD41
SiO_2	43.3	39.1	48.1	45.7	49.9
Al_2O_3	6.7	9.7	4.2	5.9	3.6
Fe_2O_3*[2]	17.0	18.6	15.3	16.3	15.6
CaO	5.6	4.4	7.9	10.6	12.6
Na_2O	4.9	4.2	9.4	9.8	8.0
K_2O	1.4	0.5	1.6	0.7	0.5
Total	78.9	76.5	86.5	89.0	89.7

Structural Formulae

Si	3.1		4.0		4.5		4.2		4.5	
Al	0.6	1.5	1.2	2.6	0.4	1.5	0.6	1.8	0.4	1.4
Fe^{+3}	0.9		1.4		1.1		1.2		1.0	
Ca	4.2		0.5		0.8		1.0		1.2	
Na	0.7	5.0	0.8	1.4	1.7	2.7	1.7	2.8	1.4	2.6
K	0.1		0.1		0.2		0.1		0.0	
Ps	-		-		-		-		-	

[1]Ps contents calculated for epidotes with near-stoichiometric formulae

[2]transitional zone plagioclase altering to epidote

Appendix Ie (cont'd.)

	B	C			D
Wt. %	A22	BB2	EA2	ED	GA1
SiO_2	35.6	37.5	37.4	37.9	37.5
Al_2O_3	22.2	24.4	23.2	24.2	23.0
Fe_2O_3*	12.4	11.9	13.5	12.3	11.7
CaO	21.9	23.3	22.3	23.4	22.9
Na_2O	0.1	0.1	0.1	0.1	0.1
K_2O	0.1	0.1	0.2	0.1	0.2
Total	92.3	97.3	96.7	98.0	95.4

Structural Formulae

Si	3.1	3.1	3.1	3.1	3.2
Al	2.3	2.4	2.3	2.3	2.3
Fe^{+3}	0.8	0.7	0.8	0.8	0.7
Ca	2.1	2.1	2.0	2.1	2.1
Na	0.0 2.1	0.0 2.1	0.0 2.0	0.0 2.1	0.0 2.1
K	0.0	0.0	0.0	0.0	0.0
Ps	-	-	-	26	23

Appendix Ie (cont'd.)

	E		F	
Wt. %	42E2	42E1	46A1	46B1
SiO_2	50.0	38.0	37.7	36.8
Al_2O_3	18.9	24.6	23.2	23.2
Fe_2O_3*	3.5	11.7	13.4	12.8
CaO	16.8	23.4	23.4	22.9
Na_2O	4.2	0.1	5.2	1.3
K_2O	0.4	0.3	0.2	0.2
Total	93.8	98.1	103.1	97.2

Structural Formulae

Si	4.1	3.1	3.0	3.1
Al	1.8	2.4	2.2	2.3
Fe^{+3}	0.2	0.7	0.8	0.8
Ca	1.5	2.1	2.0	2.0
Na	0.7 2.2	0.0 2.1	0.8 2.8	0.2 2.2
K	0.0	0.0	0.0	0.0
Ps	-	23	27	-

Appendix Ie (cont'd.)

	G		
Wt. %	PA1	PA11	PA12
SiO_2	37.5	37.1	36.7
Al_2O_3	24.6	23.9	23.0
Fe_2O_3*	11.2	12.0	12.8
CaO	22.9	22.0	22.6
Na_2O	1.2	0.1	0.1
K_2O	0.2	0.2	0.2
Total	97.6	95.3	95.4
	Structural Formulae		
Si	3.0	3.1	3.1
Al	2.4	2.4	2.3
Fe^{+3}	0.8	0.8	0.8
Ca	2.0	2.0	2.0
Na	0.2 2.2	0.0 2.0	0.0 2.0
K	0.0	0.0	0.0
Ps	-	-	-

APPENDIX II

Whole-Rock Analyses of Rocks by Electron Probe

Major element whole-rock analyses were made using an ARL automated electron probe as a macroanalyzer. Samples were ground to pass a -300 mesh standard mesh screen, and were mixed thoroughly before mounting. All powders were mounted in duplicate. The electron beam was opened to a diameter of 100 microns and numerous spots were analyzed on each of the powder mounts to obtain a valid statistical sample of the chemical variation. Precision in the analyses between duplicate powders was ±2 percent for most samples (only two samples have worse precision). The U.S.G.S. standard rock powders were ground and mounted for analysis also. These were used as standards for the powder analyses.

K-alpha lines were used in the analyses of all eight elements. Accelerating voltage was 15 KV and sample currents were 5×10^{-8} amps. Analyses of felsic rocks were made using G-2 (granite) as standard for Si, Al, Fe, Ti, Na and K, and AGV-1 (andesite) for Ca and Mg. For gabbroic and diabasic rocks, BCR-1 (basalt) standard was used to analyze for Si, Ti, Na and K, while W-1 (diabase) was used as standard for Al, Fe, Mg and Ca. Ultramafic rock analyses used the PCC-1 (peridotite) standard. Accepted values of these standard compositions (Flanagan, 1967) were used in the calculation of unknown rock compositions, using the J. W. Colby MAGIC program. Totals of the analyses

were good, in general. Most of the rocks contained hydrous minerals, so that totals of about 96 percent were common, and compare favorably to wet-chemical anhydrous totals. Some of the mafic rocks analyzed to high totals, over 101 percent, possibly due to inhomogeneity of standard powders that result in deviations from the accepted values. All analyses made using G-2 and AGV-1, even for mafic rocks, produced good totals.

Analyses of replicates of felsic rocks are listed in this Appendix. Most of these rocks contain oxidized chlorites as the only mafic mineral so total iron in these analyses has been expressed as Fe_2O_3 (Fe_2O_3*).

Appendix II

Felsic Whole-Rock Analyses

Sample	SiO_2	TiO_2	Al_2O_3	Fe_2O_3*	MgO	CaO	Na_2O	K_2O	Total
22L	63.3	1.0	16.0	4.2	1.9	3.9	5.4	0.6	96.2
22N	64.0	1.0	16.9	2.9	1.4	3.5	6.3	1.2	97.3
$22N_1$	64.5	1.2	17.0	2.9	1.5	3.6	6.4	1.0	98.1
23	58.7	1.2	17.7	4.6	2.9	5.4	5.0	0.5	96.0
23_1	59.5	1.1	17.7	5.2	3.1	5.1	5.0	0.6	97.3
25A	61.5	0.9	16.9	6.0	2.1	4.5	6.0	0.5	98.4
26	66.6	0.7	15.8	4.0	1.4	2.9	6.2	0.4	98.0
27A	64.2	0.7	17.0	4.8	1.8	3.4	5.9	0.5	98.3
27P	62.2	1.1	16.8	5.4	2.0	2.7	7.3	0.4	97.9
30A	59.5	1.0	17.3	6.6	2.5	4.9	5.7	0.4	97.9
30B	58.2	1.3	17.3	5.4	2.5	5.7	4.4	0.4	95.2
30E	60.7	1.0	16.6	4.5	2.3	5.1	5.2	0.3	95.8
30S	57.0	1.2	17.0	5.9	3.1	5.2	5.6	0.4	95.4
30SS	58.3	1.1	18.0	6.5	2.6	5.2	6.0	0.4	98.1

Appendix II (cont'd.)

Sample	SiO_2	TiO_2	Al_2O_3	Fe_2O_3*	MgO	CaO	Na_2O	K_2O	Total
321	67.2	0.7	15.8	2.8	1.2	2.3	6.1	0.4	96.5
322	65.3	0.7	15.6	3.1	1.4	3.7	5.8	0.4	96.0
323	68.9	0.3	14.6	2.0	0.8	1.4	6.9	0.3	95.2
324	70.3	0.4	15.0	1.2	0.8	1.3	6.6	0.5	95.9
325	67.2	0.5	15.6	3.9	1.6	2.0	6.2	0.4	97.4
36K	69.1	0.6	15.0	3.2	1.4	2.0	6.7	0.2	98.2
361	69.4	0.6	15.6	3.0	1.5	1.3	5.0	0.5	96.9
364	68.4	0.6	14.5	2.4	1.4	2.4	4.8	0.3	94.8
365	68.0	0.5	14.0	3.2	1.3	1.5	5.0	0.3	93.8
366	67.3	0.6	1.49	2.8	1.0	2.7	5.3	0.2	94.8
40F	66.3	0.6	15.6	4.2	2.0	2.0	6.0	0.4	97.1
401	73.1	0.5	14.7	2.4	1.0	1.9	5.8	0.3	99.7
402	66.5	0.5	15.0	4.4	2.0	1.9	5.6	0.2	96.1
403	73.4	0.5	13.9	2.0	0.9	1.6	5.8	0.2	98.3
44E	68.5	0.6	14.0	3.2	1.1	4.2	5.4	0.2	97.2
441	68.2	0.8	13.7	2.8	2.2	2.3	6.0	0.3	96.3
443	71.5	0.5	13.9	1.8	0.6	2.1	6.8	0.2	97.4
444	68.3	0.6	15.0	2.5	1.0	2.4	7.0	0.2	97.0

Appendix II (cont'd.)

Sample	SiO_2	TiO_2	Al_2O_3	Fe_2O_3*	MgO	CaO	Na_2O	K_2O	Total
48H	75.2	0.6	10.0	3.1	1.8	1.9	3.5	0.2	96.3
481	70.8	0.6	14.2	2.5	1.2	2.4	4.9	1.4	98.0
482	72.0	0.6	15.2	1.2	0.8	1.0	7.4	0.4	98.6
483	71.2	0.6	15.2	1.2	1.0	1.6	7.2	0.4	98.4
484	74.4	0.5	13.2	0.7	0.4	1.1	6.8	0.3	96.9
82	65.0	0.8	17.0	4.0	1.5	3.2	5.8	0.5	97.8
82C	68.0	0.5	15.2	3.0	1.1	3.6	4.8	0.4	96.6
831	66.9	0.4	16.0	3.0	1.4	2.2	5.9	0.5	96.3
832	60.8	0.9	17.0	4.8	2.0	3.7	5.8	0.5	95.5
834	62.6	0.7	17.3	5.0	1.4	3.5	4.8	0.5	95.9

REFERENCES

Arth, J. G., and G. N. Hanson, 1972, Quartz-diorite derived by partial melting of eclogite or amphibolite at mantle depths: Contr. Mineral. and Petrol., v. 37, p. 161-174.

Atwater, T. A., 1970, Implications of plate tectonics for the Cenozoic tectonic evolution of western North America: Geol. Soc. America Bull., v. 81, p. 3513-3536.

Auboin, J., 1965, Geosynclines: New York, Elsevier, 335 p.

Aumento, F., 1967, Magmatic evolution on the Mid-Atlantic Ridge: Earth and Planet. Sci. Lett., v. 2, p. 225-230.

——————— 1968, The Mid-Atlantic Ridge near 45° N., pt. 2 of Basalts from the area of Confederation Peak: Can. Jour. Earth Sci., v. 5, p. 1-21.

——————— 1969, Diorites from the Mid-Atlantic Ridge at 45° N: Science, v. 165, p. 1112-113.

Bailey, E. B., and W. McCallien, 1960, Some aspects of the Steinmann Trinity, mainly chemical: Geol. Soc. London Quart. Jour., v. 116, p. 365-395.

Barbat, W. F., 1971, Megatectonics of the Coast Ranges, California: Geol. Soc. America Bull., v. 82, p. 1541-1562.

Barnes, I., and J. R. O'Neill, 1969, The relationship between fluids in some fresh alpine-type ultramafics and possible modern serpentinization, western United States: Geol. Soc. America Bull., v. 80, p. 1947-1960.

Battey, M. H., 1956, The petrogenesis of a spilitic rock series from New Zealand: Geol. Mag., v. 93, p. 89-110.

Bell, J. M., E. Clarke and P. Marshall, 1911, The geology of the Dun Mountain subdivision, Nelson: Geol. Survey New Zealand Bull., v. 12, p. 1-71.

Benson, W. N., 1915, The geology and petrology of the great serpentinite belt of New South Wales: Linn. Soc. New South Wales Proc., v. 40, p. 121-173.

——————— 1926, The tectonic conditions accompanying the intrusion of basic and ultrabasic rocks: Nat. Aca. Sci. Mem., v. 19, 1st Mem., 90 p.

Blake, M. C. and E. H. Bailey, 1973, California Coast Range ophiolite--ocean ridge, marginal basin, or island arc environment? (abs.): EOS, v. 54, no. 11, p. 1219-1220.

Bischoff, A. A., 1962, The pseudotachylite of the Vredefort Dome: Geol. Soc. South Africa Trans., v. 65, p. 207-225.

Boyd, F. R., 1959, Hydrothermal investigations of amphiboles, in Abelson, P. H., ed., Researches in geochemistry: New York, John Wiley & Sons, p. 377-396.

Cameron, E. N., 1963, Structure and rock sequences of the critical zone of the eastern Bushveld complex: Min. Soc. America Spec. Paper 1, p. 93-107.

Cann, J. R., 1969, Spilites from the Carlsberg Ridge, Indian Ocean: Jour. Petrol., v. 10, p. 1-19.

——————— 1971, Petrology of basement rocks from Palmer Ridge, N. E. Atlantic: Royal Soc. Philos. Trans., v. 268, p. 605-617.

Coats, R. R., 1969, Basaltic andesites, in Hess, H. H., ed., Basalts: New York, Wiley Interscience, v. II, p. 689-736.

Coleman, R. G., 1967, Low-temperature reaction zones and alpine ultramafic rocks of California, Oregon and Washington: U. S. Geol. Survey Bull. 1247, 49 p.

——————— 1971, Plate tectonic emplacement of upper mantle peridotites along continental edges: Jour. Geophys. Res., v. 76, p. 1212-1222.

Davidson, C. F., 1967, The so-called "cognate xenoliths" of kimberlite, in Wyllie, P. J., ed., Ultramafic and related rocks: New York, John Wiley & Sons, p. 342-345.

Davies, H. L., 1968, Papuan ultramafic belt: 23rd Internatl. Geol. Cond., v. 1, p. 209-220.

——————— 1971, Peridotite-gabbro-basalt complex in eastern Papua: an overthrust plate of oceanic mantle and crust: Aust. Dept. Nat. Dev. Bur. Min. Res., Geol. Geophys. Bull., v. 128, 48 p.

Deer, W. A., R. A. Howie and J. Zussman, 1966, The rock-forming minerals, v. II of The chain silicates: London, Longmans, 379 p.

DeRoever, W. P., 1956, Sind die Alpinotypen Peridotit-massen vielleicht tektonisch verfrachtete Bruchstucke der Peridotitschale?: Geol. Rdsch., v. 46, p. 137-146.

Dewey, J. F. and J. M. Bird, 1971, Origin and emplacement of the ophiolite suite: Appalachian ophiolites in Newfoundland: Jour. Geophys. Res., v. 76, p. 3179-3206.

Dietz, R. S., 1963, Alpine serpentinites as oceanic rind fragments: Geol. Soc. America Bull., v. 74, p. 947-952.

Ernst, W. G., 1966, Synthesis and stability relations of ferrotremolite: Am. Jour. Sci., v. 264, p. 37-65.

——————— 1968, Amphiboles, Minerals, rocks and inorganic materials monographs, v. 1: New York, Springer-Verlag, 125 p.

Fairbanks, H. W., 1904, Description of the San Luis quadrangle: U. S. Geol. Survey Geol. Atlas, Folio 101, 14 p.

Fenn, P. M., 1973, Nucleation and growth of alkali feldspars from melts in the system $NaAlSi_3O_8$-$KAlSi_3O_8$-H_2O: Stanford Univ. Ph.D. thesis, 167 p.

Gass, I. G., 1967, The ultrabasic volcanic assemblage of the Troodos massif, Cyprus, in Wyllie, P. J., ed., Ultramafic and related rocks: New York, John Wiley & Sons, p. 121-134.

——————— 1968, Is the Troodos massif of Cyprus a fragment of Mesozoic ocean floor?: Nature, v. 220, p. 39-42.

Gilluly, J., 1935, Keratophyres of eastern Oregon and the spilite problem: pt. I, Am. Jour. Sci., v. 29, p. 224-252; pt. II, p. 336-352.

Green, D. H. and A. E. Ringwood, 1967, The genesis of basaltic magmas: Contr. Mineral. Petrol., v. 15, p. 103-190.

Griggs, D. T., M. S. Paterson, H. C. Heard and F. J. Turner, 1960, Annealing recrystallization in calcite crystals and aggregates, in Griggs, D. T. and J. Handin, eds., Rock deformation: Geol. Soc. America Mem. 79, p. 21-38.

Haskin, L. A., M. A. Haskin, F. A. Frey and T. R. Wildeman, 1968, Relative and absolute terrestrial abundances of the rare earths: Symp. Internatl. Assoc. Geochem. Cosmochem., Proc.: New York, Pergamon Press, p. 889-912.

Heirtzler, J. R., G. O. Dickson, E. M. Herron, W. C. Pitman III and X. LePichon, 1968, Marine magnetic anomalies, geomagnetic field reversals, and motions of the ocean floor and continents: Jour. Geophys. Res., v. 73, p. 2119-2136.

Hess, H. H., 1955, Serpentinites, orogeny and epeirogeny, in Poldervaart, A., ed., Crust of the earth: Geol. Soc. America Spec. Paper, v. 62, p. 391-408.

——————— 1960, Stillwater igneous complex, Montana: Geol. Soc. America Mem. 80, 230 p.

Hey, M. H., 1954, A new review of the chlorites: Mineralog. Mag., v. 30, p. 277-292.

Hill, M. N., 1957, Recent geophysical exploration of the ocean floor: Progr. Phys. Chem. Earth, v. 2, p. 129-163.

Holdaway, M. J., 1972, Thermal stability of Al-Fe epidote as a function of fO_2 and Fe content: Contr. Mineral. Petrol., v. 37, p. 307-340.

Hopgood, A. M., 1962, Radial distribution of soda in a pillow of spilitic lava from the Franciscan, California: Am. Jour. Sci., v. 260, p. 383-396.

Hopson, C. A. and C. J. Frano, 1973, Jurassic oceanic crustal sequence at Point Sal, California (abs.): EOS, v. 54, no. 11, p. 1220.

Hoerman, P-K and M. Raith, 1973, Formation of Al-Fe^{III} epidotes: Contr. Mineral. Petrol., v. 38, p. 307-320.

Hsü, K. J., 1969, Preliminary report and geologic guide to Franciscan mélanges of the Morro Bay-San Simeon area, California: Calif. Div. Mines and Geology Spec. Publ. 35, 46 p.

Hughes, C. H., 1972, Spilites, keratophyres and the igneous spectrum: Geol. Mag., v. 109, p. 513-527.

Irvine, T. N. and C. H. Smith, 1967, The ultramafic rocks of the Muskox intrusion, Northwest Territories, Canada, in Wyllie, P. J., ed., Ultramafic and related rocks: New York, John Wiley & Sons, p. 38-49.

Jackson, E. D., 1961, Primary textures and mineral associations in the ultramafic zone of the Stillwater complex, Montana: U. S. Geol. Survey Prof. Paper 358, 106 p.

——————— 1967, Ultramafic cumulates in the Stillwater, Great Dyke and Bushveld intrusions, in Wyllie, P. J., ed., Ultramafic and related rocks: New York, John Wiley & Sons, p. 20-38.

Jackson, E. D. and T. P. Thayer, 1972, Some criteria for distinguishing between stratiform, concentric and alpine peridotite-gabbro complexes: 24th Internatl. Geol. Cong., Comptes Rends., v. 2, p. 289-296.

Johannsen, A., 1936, A descriptive petrology of the igneous rocks, v. III: Chicago, Univ. Chicago Press, 360 p.

Karig, D. E., 1970, Ridges and trenches of the Tonga-Kermadec island arc system: Jour. Geophys. Res., v. 76, p. 239-254.

Keith, H. D. and F. J. Padden, 1963, A phenomenological theory of spherulitic crystallization: Jour. Appl. Phys., v. 34, p. 2409-2421.

Kuno, H., 1967, Mafic and ultramafic nodules from Itinome-gata, Japan, in Wyllie, P. J., ed., Ultramafic and related rocks: New York, John Wiley & Sons, p. 337-342.

Lanphere, M. A., 1973, Strontium isotopic relations in the Canyon Mountain, Oregon and Red Mountain, California ophiolites (abs.): EOS, v. 54, no. 11, p. 1220.

LePichon, X., 1969, Models and structure of the oceanic crust: Tectonophys., v. 7, p. 385-401.

Liou, J. G., 1973, Synthesis and stability relations of epidote, $Ca_2Al_2FeSi_3O_{12}(OH)$: Jour. Petrol., v. 14, p. 381-413.

Lofgren, G. E., 1968, Experimental devitrification of rhyolite glass: Stanford Univ. Ph.D. thesis, 99 p.

——————— 1974, An experimental study of plagioclase crystal morphology: Am. Jour. Sci., v. 274, p. 243-273.

Malpas, J., R. K. Stevens and D. F. Strong, 1973, Amphibolite associated with Newfoundland ophiolite: its classification and tectonic significance: Geology, v. 1, p. 45-47.

Masch, L., 1973, Untersuchungen der Aufschmelzung und Deformation der Pseudotachylite der Silvretta (Osterreich, Schweiz): Neues Jahrb. Miner. Mh., v. 11, p. 485-509.

McTaggart, K. C., 1971, On the origin of ultramafic rocks: Geol. Soc. America Bull., v. 82, p. 23-41.

Melson, W. G. and Tj. H. Van Andel, 1966, Metamorphism in the Mid-Atlantic Ridge, 22° N. latitude: Marine Geol., v. 4, p. 165-186.

Melson, W. G. and G. Thompson, 1970, Layered basic complex in oceanic crust, Romanche fracture, Equatorial Atlantic Ocean: Science, v. 168, p. 817-820.

Miyashiro, A., 1973, The Troodos ophiolitic complex was probably formed in an island arc: Earth and Planet. Sci. Lett., v. 19, p. 218-224.

Moore, J. G., 1965, Petrology of deep-sea basalt near Hawaii: Am. Jour. Sci., v. 263, p. 40-52.

Moore, J. G., R. L. Phillips, R. W. Grigg, D. W. Peterson and D. A. Swanson, 1973, Flow of lava into the sea, 1969-1971, Kilauea Volcano, Hawaii: Geol. Soc. America Bull., v. 84, p. 537-546.

Moores, E. M., 1969, Petrology and structure of the Vourinos ophiolite complex, northern Greece: Geol. Soc. America Spec. Paper 118, 74 p.

——————— 1973, Geotectonic significance of ultramafic rocks: Earth Sci. Rev., v. 9, p. 241-258.

Moores, E. M. and F. J. Vine, 1971, The Troodos massif, Cyprus and other ophiolites as oceanic crust: evaluation and implications: Royal Soc. Philos. Trans., A, v. 268, p. 443-456.

Morse, S. A., 1969, The Kiglapait layered intrusion, Labrador: Geol. Soc. America Mem. 112, 146 p.

Nicholls, G. D. and M. R. Islam, 1971, Geochemical investigations of basalts and associated rocks from the ocean floor and their implications: Royal Soc. Philos. Trans., A., v. 268, p. 469-486.

Nitsch, K-H, 1971, Stabilitatsbeziehungen von Prehnit und Pumpellyit-haltingen Paragenesen: Contr. Mineral. Petrol., v. 30, p. 240-260.

Nockolds, S. R., 1954, Chemical compositions of igneous rocks: Geol. Soc. America Bull., v. 65, p. 1007-1032.

O'Hara, M. J., 1965, Primary magmas and the origin of basalt: Scot. Jour. Geol., v. 1, p. 19-40.

——————— 1967, Mineral facies in ultrabasic rocks, in Wyllie, P. J., ed., Ultramafic and related rocks: New York, John Wiley & Sons, p. 7-17.

O'Hara, M. J. and H. S. Yoder, 1963, Partial melting of the mantle: Carnegie Inst. Wash. Yrbk., v. 62, p. 66-91.

Osborn, E. F., 1969, The complementariness of orogenic andesite and alpine peridotite: Geochim. et Cosmochim. Acta, v. 33, p. 307-325.

Pantazis, T. M., 1967, The geology and mineral resources of the Pharmakas-Kalavasos area: Cyprus Geol. Survey Mem. 8, 190 p.

Page, B. M., 1969, Relation between ocean floor spreading and structure of the Santa Lucia Range, California (abs.): Geol. Soc. America Abs. with Prog., 1969, v. 3, p. 51-52.

——————— 1972, Oceanic crust and mantle fragment in subduction complex near San Luis Obispo, California: Geol. Soc. America Bull., v. 83, p. 957-972.

Pamić, J., S. Scavnicar and S. Medjimorec, 1973, Mineral assemblages of amphibolites associated with alpine-type ultramafics in the Dinaride ophiolite zone (Yugoslavia): Jour. Petrol., v. 14, p. 133-157.

Pearce, J. A. and J. R. Cann, 1971, Ophiolite origin investigated by discriminant analysis using Ti, Zr and Y: Earth and Planet. Sci. Lett., v. 12, p. 339-349.

Penrose Conference, 1972, Ophiolites: Geotimes, v. 17, p. 24-25.

Pessagno, E. A., 1973, Age and geologic significance of radiolarian cherts in the California Coast Ranges: Geology, v. 1, p. 153-158.

Raitt, R. W., 1963, The crustal rocks, in Hill, ed., The sea, 3: New York, John Wiley & Sons, p. 85-102.

Reinhardt, B. M., 1969, On the genesis and emplacement of ophiolites in the Oman mountains geosyncline: Schweiz. Min. Petrog. Mitt., v. 49, p. 1-30.

Ringwood, A. E., 1969, Composition of the crust and upper mantle, in Hart, S., ed., The earth's crust and upper mantle: Am. Geophys. Union Mon. 13, p. 1-17.

Smith, C. H., 1958, Bay of Islands igneous complex, western Newfoundland: Can. Geol. Survey Mem. 290, 132 p.

Snoke, A. W., 1972, Petrology and structure of the Preston Peak area, Del Norte and Siskiyou Counties, California: Stanford Univ. Ph.D. thesis, 274 p.

Southwick, D. L., 1974, Geology of the alpine-type ultramafic complex near Mount Stuart, Washington: Geol. Soc. America Bull., v. 85, p. 391-402.

Steinmann, G., 1905, Geologische Beobachtungen in den Alpen II: Die Schardt'sche Uberfaltungstheorie und die geologische Bedeutung der Tiesfeeabsatze und der ophiolithischen Massengesteine: Ber. Nat. Gesell. Freiburg. i. Bd., v. 16, p. 44-65.

——————— 1927, Die ophiolitischen Zonen in den mediterranean Kettengebirgen: 14th Internatl. Geol. Cong., Comptes-Rends., p. 637-667.

Steuber, A. M. and V. R. Murthy, 1966, Strontium isotope and alkali element abundances in ultramafic rocks: Geochim. et Cosmochim. Acta, v. 30, p. 1243-1259.

Thayer, T. P., 1960, Some critical differences between alpine-type and stratiform peridotite-gabbro complexes: 21st Internatl. Geol. Cong., v. 13, p. 247-259.

——————— 1963, The Canyon Mountain complex, Oregon, and the alpine mafic magma stem: U. S. Geol. Survey Prof. Paper 475-C, p. C82-C85.

——————— 1969, Peridotite-gabbro complexes as keys to petrology of mid-ocean ridges: Geol. Soc. America Bull., v. 80, p. 1515-1522.

Thayer, T. P. and G. R. Himmelberg, 1968, Rock succession in the alpine-type mafic complex at Canyon Mountain, Oregon: 23rd Internatl. Geol. Cong., v. 1, p. 175-186.

Turner, F. J. and J. Verhoogen, 1960, Igneous and metamorphic petrology: New York, McGraw-Hill Book Co., 694 p.

Vallance, T. G., 1960, Concerning spilites: Linn. Soc. New South Wales Proc., v. 85, p. 8-52.

——————— 1965, On the chemistry of pillow lavas and the origin of spilites: Mineralog. Mag., v. 34, p. 471-481.

Wager, L. R. and G. M. Brown, 1968, Layered igneous rocks: London, Oliver and Boyd, 588 p.

Wenner, D. B. and H. P. Taylor, 1973, Oxygen and hydrogen isotope studies of the serpentinization of ultramafic rocks in oceanic environments and continental ophiolite complexes: Am. Jour. Sci., v. 273, p. 207-239.

Wetzel, R., 1973, Chemismus und physikalische Parameter einiger Chlorite aus der Grönschieferfazies: Schweiz. Min. und Pet. Mitt., v. 53, p. 273-298.

Williams, H. and J. Malpas, 1972, Sheeted dikes and brecciated dike rocks within transported igneous complexes, Bay of Islands, Newfoundland: Can. Jour. Earth Sci., v. 9, p. 1216-1229.

Wilshire, H. G., 1971, Pseudotachylite from the Vredefort ring, South Africa: Jour. Geology, v. 79, p. 195-206.

Wilshire, H. G. and R. A. Binns, 1961, Basic and ultrabasic xenoliths from volcanic rocks of New South Wales: Jour. Petrol., v. 2, p. 185-208.

Wilshire, H. G., C. E. Meyer, E. C. Schwarzman and L. C. Calk, 1974, Ultramafic xenoliths from western United States (abs.): Geol. Soc. America Abs. with Prog., v. 6, p. 483.

Wyllie, P. J., 1967, Petrography and petrology, in Wyllie, P. J., ed., Ultramafic and related rocks: New York, John Wiley & Sons, p. 1-6.

Yoder, H. S., 1967, Spilites and serpentinites: Carnegie Inst. Wash. Yrbk., v. 65, p. 269-279.

Yoder, H. S. and C. E. Tilley, 1962, Origin of basalt magmas: an experimental study of natural and synthetic rock systems: Jour. Petrol., v. 3, p. 342-532.

WERT
BOOKBINDING
MIDDLETOWN, PA.
AUG. 84
We're Quality Bound